6-3-2004

Comparing Twenty-Four Years of Forest Change in Two Communities of Mexico's Meseta Purépecha Using Multi-Spectral Satellite Imagery

Kevin Scott Martin
Portland State University

Follow this and additional works at: https://pdxscholar.library.pdx.edu/open_access_etds

Part of the Demography, Population, and Ecology Commons, Physical and Environmental Geography Commons, and the Remote Sensing Commons

Let us know how access to this document benefits you.

THESIS APPROVAL

The abstract and thesis of Kevin Scott Martin for the Master of Science in Geography
were presented June 3, 2004, and accepted by the thesis committee and the
department.

COMMITTEE APPROVALS:

_____
Andrew G. Fountain, Chair

_____
Keith S. Hadley

_____
Martha A. Works

_____
Alan Yeakley
Representative of the Office of Graduate Studies

DEPARTMENT APPROVAL:

Teresa Bulman, Chair
Department of Geography

ABSTRACT

An abstract of the thesis of Kevin Scott Martin for the Master of Science in Geography presented June 3, 2004.

Title: Comparing Twenty-Four Years of Forest Change in Two Communities of Mexico's Meseta Purépecha Using Multi-Spectral Satellite Imagery.

The Meseta Purépecha, a volcanic plateau in the Mexican state of Michoacán, is home to one of the most species-rich pine forests in the world. Recent increases in demand for forest products has put added pressure on these resources. Though existing research has suggested significant deforestation in the Meseta, there is little information identifying specific areas of decline. This study focuses on two indigenous communities in the Meseta—Pichátaro and Sevina. Both communities have long relied on wood as an economic resource. However, the two communities have reacted differently to increased demand for forest resources. The purpose of this study is to identify the differences in the rate and extent of forest change between Pichátaro and Sevina.

Three dates of Landsat satellite images – 1976, 1986, and 2000 – were used to identify changes in the Meseta's forests. Supervised classification was used to classify the 2000 image into forested and non-forested areas. Change detection was performed on the 1976 through 2000 images to identify areas of forest clearing and forest

regrowth. The 2000 image was then used as a reference for generating maps of historic forest extent based on the change detection results.

Results show that between 1986 and 2000, Sevina cleared approximately 16% of its forested land between while Pichátaro experienced a net gain of 7%. In the same period, 93% of the deforestation in the combined study area occurred within the community boundary of Sevina, which manages only 35% of the study area forests. Sevina's remaining forests are also more isolated and fragmented than the forests of Pichátaro. The differences between the two communities appear related to management practices. Sevina has relied on larger-scale timber harvesting to derive economic benefits from its forests. Pichátaro has focused on local harvesting and value-added production.

COMPARING TWENTY-FOUR YEARS OF FOREST CHANGE IN TWO

COMMUNITIES OF MEXICO'S MESETA PURÉPECHA USING MULTI-

SPECTRAL SATELLITE IMAGERY

by

KEVIN SCOTT MARTIN

A thesis submitted in partial fulfillment of the
requirements for the degree of

MASTER OF SCIENCE
in
GEOGRAPHY

Portland State University
2005

ACKNOWLEDGEMENTS

TABLE OF CONTENTS

LIST OF TABLES

LIST OF FIGURES

CHAPTER 1: INTRODUCTION

Forest resources play a central role in the regional economy of communities in the Meseta Purépecha region of Michoacán, Mexico (Works and Hadley, 2004). Recent increases in global demand for Mexico's forest products resulting from the passage of trade agreements such as North American Free Trade Agreement (NAFTA) and General Agreement on Tariffs and Trade (GATT) has put increased pressure on the forests of the Meseta (Jaffee, 1996). Though existing research has suggested widespread deforestation and environmental degradation in the Meseta Purépecha region (Alvarez-Icaza *et al.*, 1993), little information exists regarding specific areas of forest decline. Even less understood are the changes in forest structure and health resulting from intensive local harvesting. In many areas of the Meseta older stands are being replaced by younger, fragmented forests. Furthermore, because these forests are communally owned and managed, the rates and patterns of forest change vary by jurisdiction.

The Meseta is home to some of the most diverse pine forests in North America (Watts and Bradbury, 1982; Perry, 1991; Styles, 1993). These forests have played a particularly important role in shaping local economies. The people of the Meseta, including a large indigenous Purépecha population, have long relied on pine as a source of fuel and for the manufacturing of products such as furniture, railroad ties, and avocado crates (Works and Hadley, 2004). These items are produced for domestic use and foreign export.

1

As in other indigenous areas of Mexico, the forests of the Meseta are communally owned and managed. Local control of forests is the result of agrarian reforms occurring after the Mexican revolution (1910-1920) (Jaffee, 1996). This type of community-based management can lead to significant differences in the patterns and rates of forest change between jurisdictions. For example, the deregulation of avocados under NAFTA (1994) has accelerated the rate of deforestation in communities where lumber is harvested primarily for avocado crate production (Jaffee, 1996).

Pichátaro and Sevina are two of the indigenous *communidades* in the Meseta that have long relied on wood as an economic and cultural resource. However, the communities have responded differently to the increased demand for forest resources. Sevina (Figure 1.1) has focused on larger-scale commercial clearing of its forests, and has largely exported the timber unprocessed. This is partially a result of Sevina's cultural and geographic orientation towards the western Meseta, including the communities of Cherán and Uruapan, a center for avocado cultivation (Works and Hadley, 2004). Sevina has been largely isolated from the tourist market centered around Lake Pátzcuaro in the eastern Meseta, and has therefore not experienced the same demand for local crafts as neighboring Pichátaro. Though the community has recently undertaken a federally-funded replanting effort designed to replace clear-cut stands, little intact forest remains, leading to a collapse of the local timber industry (Works and Hadley, 2004).
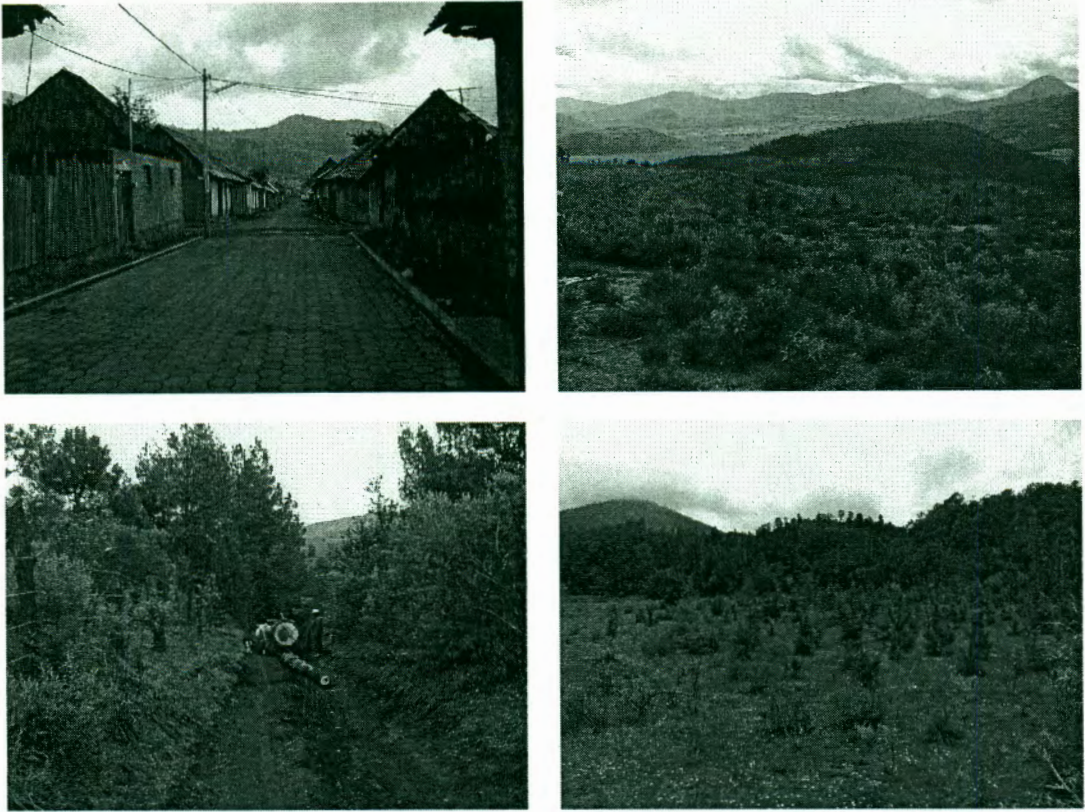
Figure 1.1. Clockwise from top left—town of Sevina, view of forested areas above town, replanted area, lumber extraction with traditional oxcart.

Pichátaro (Figure 1.2) has been more successful in maximizing the value of forest resources to the community. Its management style more closely adheres to the "community forest enterprise" (CFE) model developed in the early 1980's by indigenous communities in the state of Oaxaca. The CFE model focuses on community control of forest harvesting, setting up local sawmills to add value to unprocessed logs, and investing the proceeds from forest resources in the community (Jaffee, 1996). Unlike Sevina, Pichátaro processes its timber in small, locally owned

3
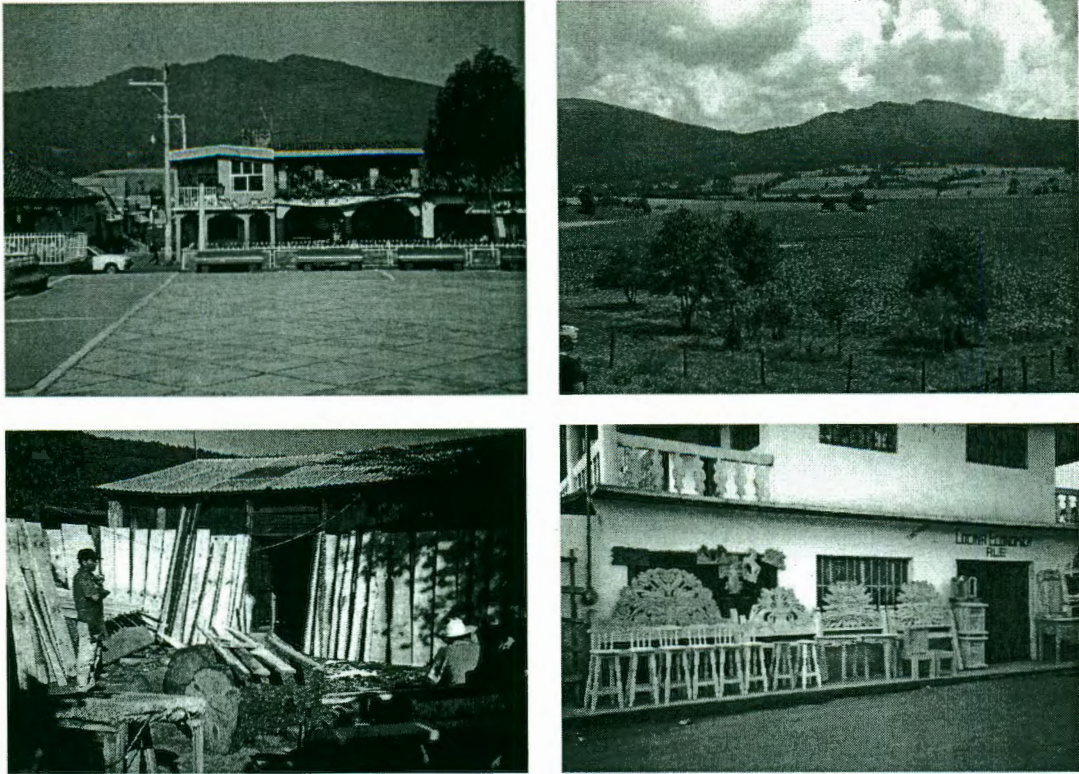
Figure 1.2. Clockwise from top left—town of Pichátaro, view of forested areas south of town, examples of pine furniture, private lumber mill.

and operated mills. Local workshops use the processed wood to create a variety of furniture items—such as tables, chairs, and decorative wood carvings—that are sold locally and exported to other areas of Mexico (Chase, 2003).

Though both communities are aware of deforestation and view it as problematic, there has not been any effort to formally measure the rate or extent of deforestation. Furthermore, the existing maps of regional forests are outdated and unreliable. A map of forested areas could be developed using extensive field-sampling and other ground-based techniques. However, it would be very difficult to reconstruct past forest extent.

4

Satellite imagery offers a cost-effective solution. Both the present and past forest conditions can be mapped using a series of automated techniques to classify the images into general land-cover categories. Changes in land-cover can then be measured from one image date to the next.

The purpose of this study is to quantify the extent and pattern of forest clearing and forest regrowth in the communities of Sevina and Pichátaro using Landsat images collected in 1976, 1986, and 2000. The 2000 image is processed to reduce the effect of topography and then classified into general land-cover categories. An automated change detection method is used to identify landscape change between 1976 and 2000. The 2000 classification and change detection results serve as the reference for mapping the extent of communal forests in 1976 and 1986. The resulting forest maps are then compared to identify the pattern and rate of forest change in the period between 1976 and 2000. Forest change is examined by community to determine whether the different management practices of Sevina and Pichátaro have resulted in significant differences in the overall extent and health of their respective forests. Because Pichátaro has not used large-scale clear-cutting operations and employs more sustainable selective-harvesting methods, the community should have experienced less forest clearing in the last few decades than Sevina.

This study is part of a larger project focusing on how the political and economic climates of the Meseta influence forest resource consumption and vice versa (Works and Hadley, 2001; Chase, 2003; Works and Hadley, 2004). The ultimate goal of this broader effort is to better understand how diminishing forest resources play a role in

shaping the cultural landscape of Sevina and Pichátaro as each community responds to local, regional, national and global demand for forest products (Works and Hadley, 2001). Accurately identifying the extent of forest change in each community is a key factor in being able to analyze and understand these relationships.

CHAPTER 2: STUDY AREA

The Meseta Purépecha is located in the north-central portion of the state of Michoacán, Mexico (Figure 2.1). The Meseta is a high-elevation plateau consisting of a series of flat-bottomed valleys averaging 2200 m above sea level. The valleys are surrounded by cinder cones and pyroclastic volcanoes that rise to 3500 m (Garcia and Alvarez, 1994; Mas and Ramirez, 1996). The climate is sub-humid temperate with monthly temperatures ranging from approximately 17°C to 24°C. The period between April and June is the warmest. Annual rainfall is approximately 813mm (32 in.), over 75% of which occurs during the June to September rainy season. July is the wettest month, with 191mm (7.5 in.) of precipitation on average.

Lake Pátzcuaro, about 11 km due east of Pichátaro, is the only major hydrologic feature in the Meseta. The lake basin has long been a center for settlement and agriculture (Works and Hadley, 2004). The Spanish-colonial city of Pátzcuaro, just south of the Lake, serves as a tourist destination for both domestic and foreign travelers.

The forests of the region are dominated by multiple species of pine (*Pinus pseudostrobus, P. leiophylla, P. michoacana, P. teocote, P. montezume,* and *P. oocarpa* are the most commonly found species). The pine forests of the Meseta have been recognized as some of the most species-rich in the world (Watts and Bradbury, 1982; Perry, 1991; Styles, 1993). Fir (*Abies religiosa*) mixes with pine at higher elevations, becoming dominant only above 3000 m (Velázquez *et al.,* 2000). A

Figure 2.1. Relative location of study area.

mixture of pine and oak woodland (*Quercus laurina* and *Q. crassfolia* are common species of oak) is the most abundant forest type in the Meseta, with pine the dominant species everywhere but the lowest elevations (Velázquez *et al.,* 2000). Alder (*Alnus arguta, A. firmofilia, A. jorullensis*) is present in most areas as a subdominant species (Watts and Bradbury, 1982). The pine and mixed-pine forests of the Meseta have been heavily cultivated for lumber and firewood, and little remnant forest remains. Larger pines often have numerous scars from resin tapping—pine resin is extracted to make turpentine—though this does not appear to have a substantial effect on tree mortality

8
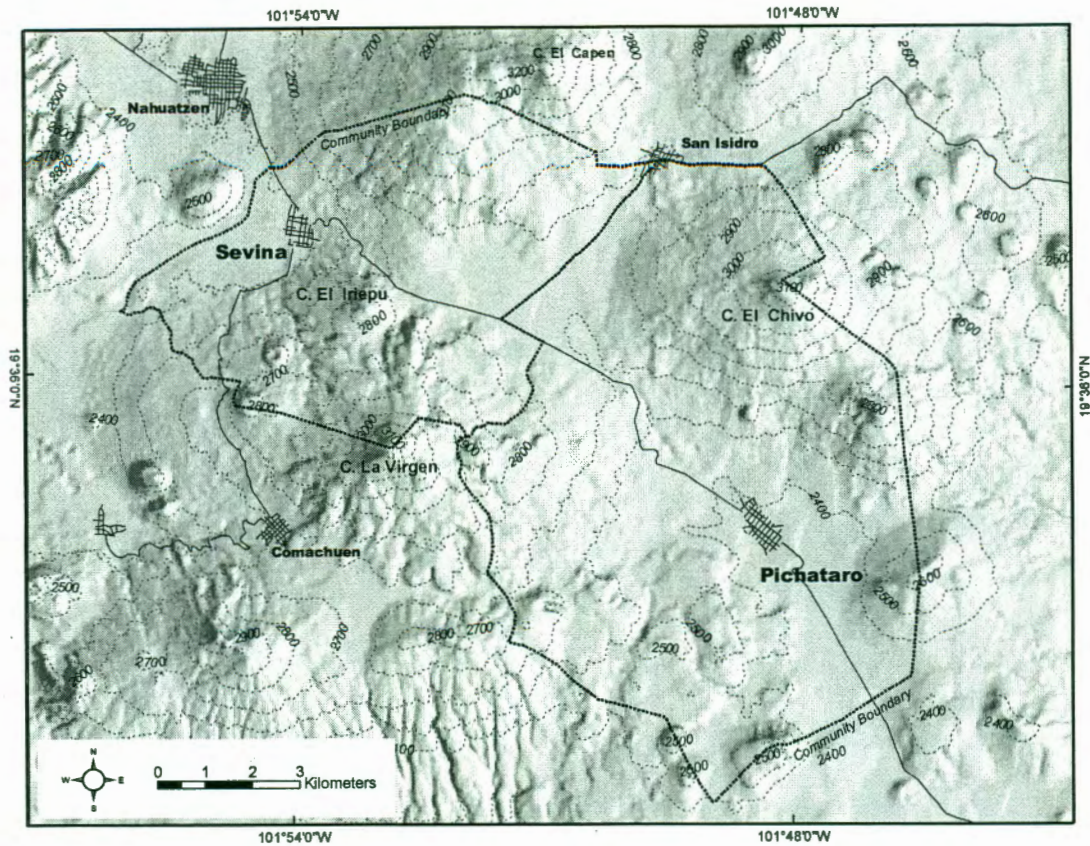
Figure 2.2. Community boundaries of Sevina and Pichátaro shown over a shaded-relief map (Study Area).

(Styles, 1993). Agriculture (maize) and pasture are confined primarily to the valley floor.

The community of Sevina sits in a narrow valley between the mountains of Campo El Capen (approximately 3350 m) and Cerro El Iriepu (~2850 m) at an elevation of ~2400 m (Figure 2.2). Sevina manages forests within an area covering approximately 4713 hectares. According to the most recent population data available, an estimated 2700 residents live in or around the community (INEGI, 2000).

Pichátaro, 12 km to the southeast of Sevina, is in the central portion of a wide valley framed by the peaks of Cerro El Chivo (~3250 m) and Cerro La Virgen (~3310 m). Like Sevina, the town sits at an elevation of ~2400 m. Its communal area is significantly larger than that of Sevina, at approximately 8609 ha. An estimated 5000 individuals live in or near Pichátaro (INEGI, 2000).

CHAPTER 3: METHODS

Several studies have demonstrated the utility of multi-spectral satellite image classification for determining the rate of deforestation, and to a lesser degree, the degradation over time of forested areas (Running *et al.*, 1986; Garcia and Alvarez, 1994; Cohen *et al.*, 1995; Cohen *et al.*, 1998; Mas, 1999). However, many have focused on low elevation areas and have restricted their analysis to regions of relatively low relief to reduce the disrupting influences of surface topography and shadow on the spectral response of surface features (the brightness of objects over a range of wavelengths) (Campbell, 1996; Keating, 1997). The fact that many forested landscapes are topographically variable makes this a notable limitation. Remote sensing research has demonstrated the value of topographic normalization for improving the accuracy of classification in mountainous areas (Smith *et al.*, 1980; Leprieur *et al.*, 1988; Civco, 1989; Colby, 1991; Colby and Keating, 1998). Topographic normalization uses mathematical techniques to reduce the influence of terrain on the measured brightness of surface features.

Few studies have examined the subtropical temperate forests of Mexico. Mas and Ramirez (1996) studied the feasibility of digital image classification for mapping the 1992 canopy cover in a portion of the Meseta. They found that the limitations of the historic reference maps and other ancillary data resulted in relatively low classification accuracy with only 67% of the study area's land-cover correctly identified. However, a variety of techniques have been developed and tested elsewhere to automatically

detect land-cover change using a direct comparison of multi-temporal satellite data, overcoming the effect of poor or nonexistent reference data on the accuracy of historic image classification (Jensen, 1996; Mas, 1999; Hayes and Sader, 2001). The results of this type of change detection can also be used to map the historic extent of a land-cover type, such as forested areas, by using a classified base year image as reference (Pilon *et al.*, 1988; Yuan *et al.*, 1998).

Data Sources

Four Landsat satellite images of the study area were used in this study—a 1976 Multi-spectral Scanner (MSS) image, a 1986 MSS image, a 1986 Thematic Mapper (TM) image, and a 2000 Enhanced Thematic Mapper Plus (ETM+) image (Appendix). Both 1986 images were collected at the same day and time by the Landsat 5 satellite, which carries an operational MSS and a TM sensor. The ETM+ image was collected by the Landsat 7 satellite. Sun angle and seasonal vegetation differences are minimal because the images were acquired at about the same time of day and within the three week period between March 28 and April 20 (Jensen, 1996) (Table 3.1).

Table 3.1. Satellite image acquisition information.

Image Date	Image Time	Solar Elevation	Solar Azimuth	Sensor
March 28, 1976	16:24	50°	111°	MSS
April 6, 1986	16:37	55°	108°	MSS
April 6, 1986	16:37	55°	108°	TM
April 20, 2000	17:04	64°	105°	ETM+

The MSS, TM and ETM+ images underwent basic radiometric and geometric correction by the USGS EROS Data Center. The USGS radiometric correction adjusts the brightness of the satellite image to correct for sensor inconsistency and image brightness anomalies (USGS, 2004). The geometric correction applied by the USGS corrects for "systematic" geometric error introduced by factors such as the rotation of the Earth and changes in the speed of the satellite (USGS, 2004). Systematic error can be measured and removed without the need for identifying ground-control point (GCP) locations on the surface (Jensen, 1996). This type of correction results in images with a horizontal accuracy of +/- 250 m. The MSS images were part of a larger series of images processed and made available as part of the North American Landscape Characterization Project (NALC). The NALC images went through additional processing that included improved geometric correction and co-registration of the images, resulting in a horizontal accuracy of +/- 30 m or less (Lunetta *et al.*, 1993).

Past studies have highlighted the difficulty of comparing MSS and TM/ETM+ imagery due to the sensor differences (Jensen, 1996; Yuan *et al.*, 1998). Land-cover features distinct in TM and ETM+ imagery may not be distinct in an MSS image because of the latter's lower spatial resolution, which is determined by the size of the fundamental picture elements, known as pixels, that make up a digital image (Table 3.2). The sensors have different spectral resolutions as well, meaning they record energy in different portions of the electromagnetic spectrum. Land-cover distinguishable in the portion of the spectrum recorded by one sensor may escape

Table 3.2. Summary of Landsat MSS/TM sensor characteristics.

Sensor	Original Launch Date	Spatial Resolution	Spectral Resolution	Radiometric Resolution
MSS	June 23, 1972	76 m^2	Band 1: 0.5-0.6 μm (green)	0 to 127
			Band 2: 0.6-0.7 μm (red)	
			Band 3: 0.7-0.8 μm (near infrared)	
			Band 4: 0.8-1.1 μm (near infrared)	
TM	July 16, 1982	30 m^2	Band 1: 0.45-0.52 μm (blue-green)	0 to 255
			Band 2: 0.52-0.60 μm (green)	
			Band 3: 0.63-0.69 μm (red)	
			Band 4: 0.76-0.90 μm (near infrared)	
			Band 5: 1.55-1.75 μm (mid infrared)	
			Band 7: 2.08-2.35 μm (mid infrared)	
		120 m^2	Band 6: 10.4-12.5 μm (thermal infrared)	
ETM+	April 15, 1999	30 m^2	Band 1: 0.45-0.52 μm (blue-green)	0 to 255
			Band 2: 0.53-0.61 μm (green)	
			Band 3: 0.63-0.69 μm (red)	
			Band 4: 0.78-0.90 μm (near infrared)	
			Band 5: 1.55-1.75 μm (mid infrared)	
			Band 7: 2.09-2.35 μm (mid infrared)	
		60 m^2	Band 6: 10.4-12.5 μm (thermal infrared)	
		15 m^2	Band 8: 0.52-0.90 μm (panchromatic)	

detection by another sensor with a more limited spectral resolution (Jensen, 1996).

The MSS and TM/ETM+ sensors also have different radiometric resolutions (the

range of digital values that the sensor can store). It is therefore difficult to accurately

determine whether differences between an MSS and a TM image are the result of

actual changes in land-cover or are a consequence of sensor differences. These

complications can be minimized by only comparing data from a single sensor series

(Yuan *et. al.*, 1998). Despite some slight differences in the spectral sensitivity of the

bands, Landsat TM and ETM+ are generally considered part of the same sensor series

and can be directly compared for change detection purposes (Yuan *et. al.*, 1998;

Change Detection Study

Start Date ◄──────────────────────────────────► End Date

Landsat 4,5
MSS data compared with ◄──► MSS Image
TM Image ◄──► *compared with TM/ETM+ data*

Figure 3.1. Using Landsat 4,5 data to incorporate MSS data in change detection studies.

USGS, 2004). The TM/ETM+ thermal-infrared bands (Band 6) are generally not

considered applicable to vegetation classification (Campbell, 1996; ERDAS, 1999)

and are not used in this study.

Landsat 4 and 5 were configured to acquire simultaneous images with both the

MSS and TM sensor, providing a single date and time of imagery in both MSS and

TM formats. Having MSS and TM images from the same date allows older MSS data

to be incorporated into change detection studies without having to directly compare it

to TM or ETM+ data (Figure 3.1). For the purpose of this study, the 1976 MSS image

can be compared with the 1986 MSS image, and the 1986 TM image can be compared

with the 2000 ETM+ image.

A set of 1:50000-scale digital geographic data was received from the Instituto

Nacionál de Estadística, Geografía y Informática (INEGI). The dataset, depicting

roads, elevation contours and community boundaries in 1999, provided the reference

for registering aerial photos and satellite imagery. A 50-meter DEM of the study area

was included with the INEGI dataset. The DEM was resampled to 30 meters in

ERDAS Imagine image processing software using a bilinear interpolation technique so

15

that it matched the resolution of the 1986 and 2000 Landsat data. Resampling the DEM reduced the likelihood of geometric error introduced by the resolution differences between the elevation model and the satellite imagery (ERDAS, 1999).

Two sets of unrectified aerial photographs covering a portion of the study area, taken in 1974 (1:30000) and 1990 (1:50000), were also received from INEGI. All photographs were scanned and geographically rectified in ArcGIS GIS software based on visible road intersections. Forest stand maps produced by the Comisión Forestal del Estado de Michoacán in 1985 and 1994 were also digitized in ArcGIS. The aerials and stand maps served as reference for locating field sample plots and for refining reference areas used for topographic normalization and image classification

Field Data Collection

I completed my field data collection for this study in August 2000. The field crew consisted of myself and three others conducting similar research in the Meseta (Works and Hadley, 2001; Chase, 2003; Works and Hadley, 2004). The main goal of the field effort was to create a representative sample of the different forest stand types in the study area. This sample was used to classify the April 2000 satellite image.

We established twenty circular sample plots ranging in size from 125 m^2 to 2000 m^2 within the forest management areas of Sevina and Pichátaro (Works and Hadley, 2004) using techniques described by Hadley and Savage (1996) (Figure 3.2). Plot size was based on the number of trees in the sample plot area, with each plot including a minimum of 20 live trees. We established ten plots in each community. The plots were
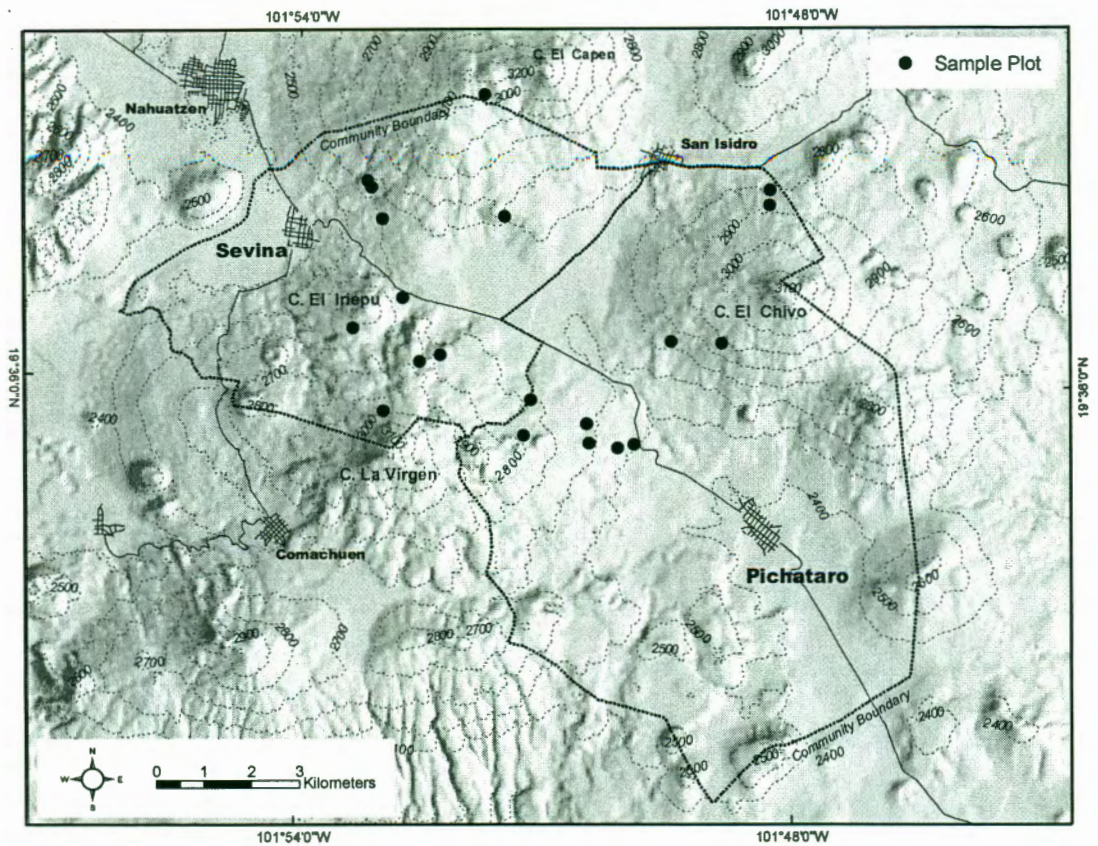
Figure 3.2. Sample plot locations.

subjectively located based on the knowledge of local guides, accessibility of the stand, and information from the 1985 and 1994 stand maps. We located the plots in stands of different ages, canopy and tree densities, and species composition in order to be as representative of the regional forest as possible (Oderwald and Wynne, 2000). However, the diversity of forest conditions, limited accessibility, and recent logging did not allow sampling of the entire range of local forest types. Field sampling therefore focused on establishing plots in a broad range of pine and mixed pine stands.

17

The center of each sample plot was mapped using an average of 10 minutes of Global Positioning System (GPS) point data collected at 5 second increments. This resulted in a horizontal accuracy of approximately +/- 5 m (Refan and Mohammadi, 2001). Trees in each plot were located using their distance and azimuth from the plot center point. All trees were identified by species or genus and the diameter at breast height (DBH) was measured. Seedlings and saplings <5 cm in diameter and <1.5 m tall were not mapped. At least 5 pine trees in each plot were cored to determine tree age. The number of rings in each core was counted in the field by at least two members of the field team to ensure an accurate count. The height and approximate crown diameter of a selection of trees within the plot was measured using a laser range-finder. Digital photos of each plot and of the above canopy closure (as visible from the ground) were also collected.

A "stand sample" area representing the forest type of each sample plot was identified to capture a larger area of homogeneous vegetation than the sample plot itself represented. This stand sample was delineated in the field based on the visual observations of the field crew. GPS positions were collected at 5 second intervals while a portion of the stand surrounding a plot was circumnavigated on foot. Because these GPS points were not averaged at each collection location, horizontal accuracy was reduced to approximately +/- 15 m (Refan and Mohammadi, 2001). The GPS points were manually connected in ArcGIS to delineate the forest stand sample (Figure 3.3). The same technique was used to identify areas of non-forested land-cover such as agriculture and low-structure shrubby vegetation. In areas with poor GPS
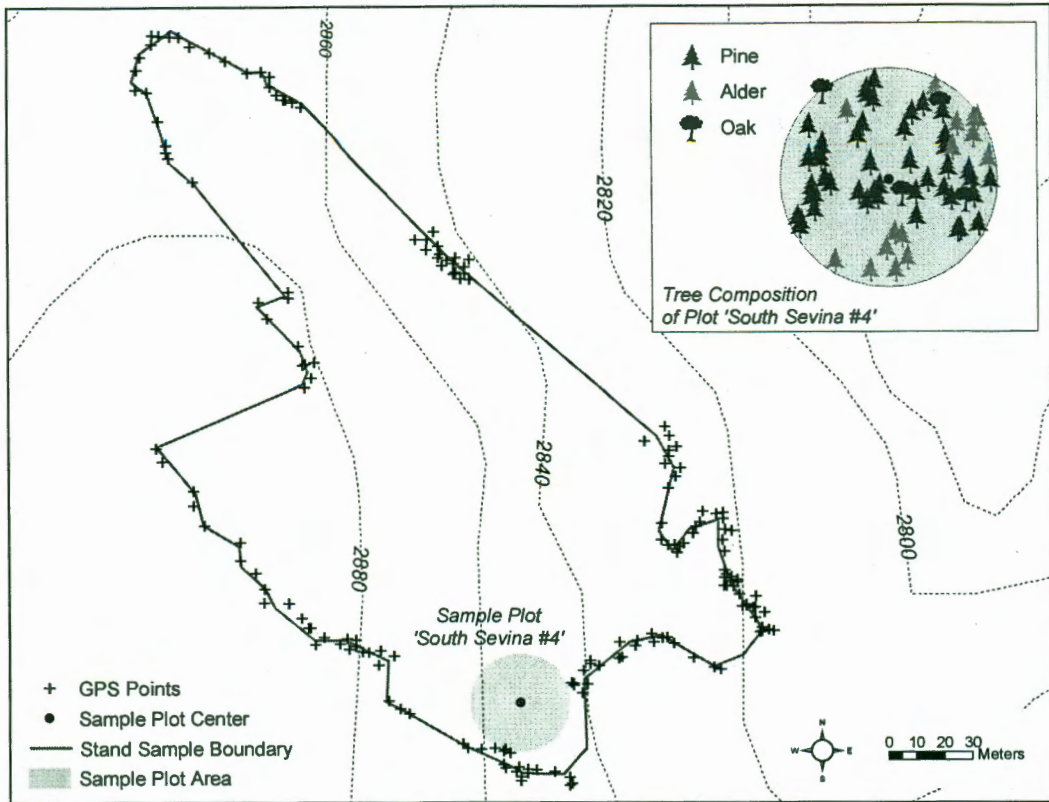
Figure 3.3. Sample plot and stand sample for site 'South Sevina #4.'

satellite coverage or topographic interference, the stand sample boundaries were

visually interpolated using available GPS points and the 2000 ETM+ image as

reference.

I used DBH as the independent variable in a linear regression to predict age, crown

diameter, and tree height for pine trees where that information was not collected in the

field (Table 3.3). The relationship between DBH and crown diameter and tree height

was strong; tree age was slightly less predictable though sufficient for producing a general description of the plot.

Table 3.3. Linear regression results by tree parameter with diameter at breast height, d, as the independent variable (pine only).

Dependent Variable	Equation	r^2	Standard Error	Sample Size
crown diameter	D = 1.44 + 0.22d	0.84	2.51	65
tree height	H = 8.62 + 0.34d	0.82	4.66	105
tree age	A = 10.69 + 0.68d	0.67	12.71	99

Summary statistics for each plot were generated, and the plot and its surrounding stand were categorized into a dominant and subordinate genus based on canopy dominance, density of trees, and the stand basal area of each genus. Basal area is the measure of the standing tree volume in a given plot or stand, usually in square meters per hectare (Table 3.4). Basal area (BA) for each sample plot (s) is calculated as:

$$BA_s = \frac{\sum_{t=1}^{N} \pi \left(\frac{DBH_t}{200} \right)^2}{a_s} \tag{1}$$

where N is the total number of trees of a specific genus within the plot, DBH is the measured or predicted diameter-at-breast-height in centimeters for each tree (t) of a specified genus within the plot, and a is the plot area of sample plot s in hectares.

Table 3.4. Example of sample plot statistics (plot Sevina South #4).

GENUS	Total Number	% in Dominant Canopy	% in Mid Canopy	% in Sub Canopy	Density (Trees/ha)	Mean DBH (cm)	Basal Area (m²/ha)	Mean Age (years)
Pinus	46	0.0%	19.6%	80.4%	460	11.76	6.50	19.33
Quercus	2	100.0%	0.0%	0.0%	20	75.50	9.30	N/A
Alnus	15	0.0%	20.0%	80.0%	150	16.60	4.00	N/A
Abies	0	0.0%	0.0%	0.0%	0	0.00	0.00	N/A

Overview of Image Processing Methodology

The satellite imagery was processed in multiple ways to meet the objectives of my study (Figure 3.4). Before classification and change detection were performed, I applied additional radiometric and geometric corrections to improve the spatial and spectral accuracy of the images. All image dates were orthorectified and co-registered using the DEM and a set of user-defined control points. In addition, I applied two types of spectral correction to the imagery. A radiometric normalization was applied to all image dates to reduce the brightness variation in the images over time. A non-Lambertian topographic normalization technique was applied to the orthorectified 2000 ETM+ to reduce the effects of topography on pixel brightness.

The topographically normalized 2000 image was used as the input into a supervised classification to map land-cover in April of 2000. The radiometrically normalized 1976, 1986 and 2000 images were input into an automated change detection process to classify areas of forest clearing and forest regrowth using a "Kappa thresholding" technique. I used the 2000 supervised classification and 1976/1986 and 1986/2000 change classification images as reference for temporally-
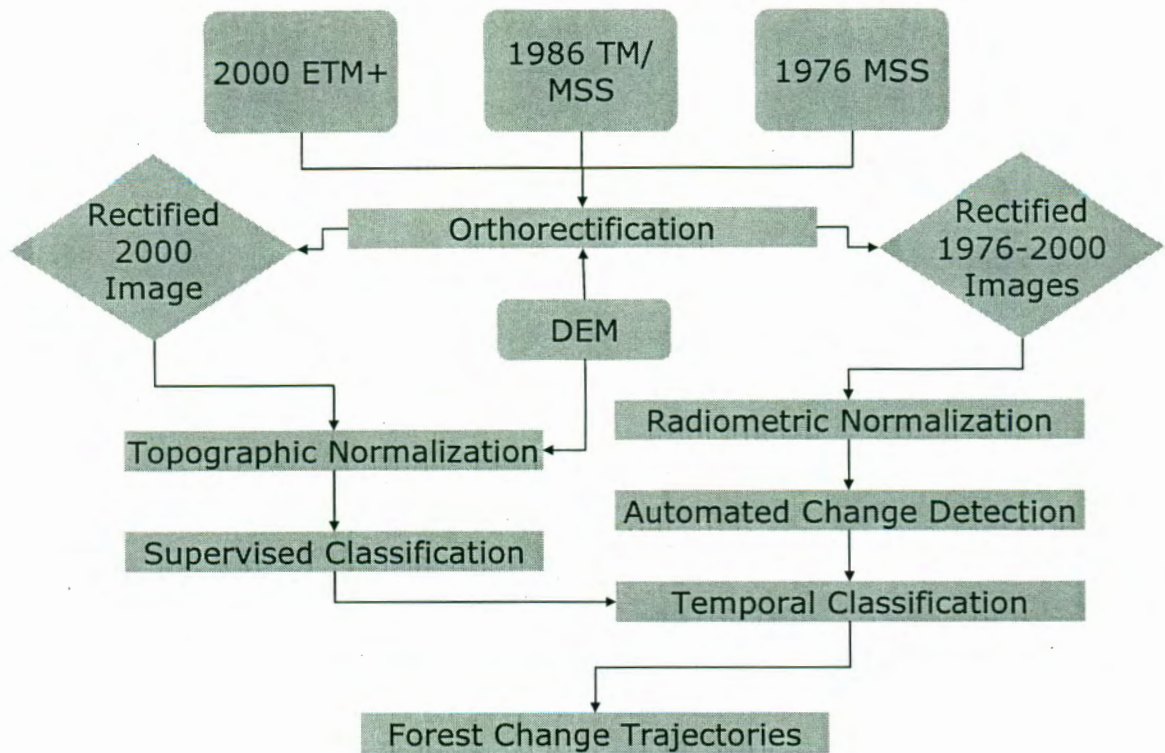
Figure 3.4. Overview of image processing methodology.

classifying the historic forest extent in 1986 and 1976. The maps of forest extent were

combined to create forest change trajectories for the 1976 to 2000 time period. Finally,

I calculated landscape metrics for the forest extent maps and the forest change

trajectories to quantify the spatial pattern of forest change. Each of these steps is

described in detail in the following sections.

Image Data Pre-Processing

Image Orthorectification

The 2000 Landsat image was orthorectified in ERDAS Imagine using the DEM as vertical reference and 12 digitized road intersections as horizontal control points. Orthorectification uses a sensor-specific algorithm to systematically reduce the effects of terrain displacement and sensor orientation on the geometric accuracy of the image while georeferencing the image to a set of user-defined ground control points (ERDAS, 1999). The 1986 and 1976 images were subsequently orthorectified using the corrected 2000 image as reference. Because the 1986 and 1976 MSS images had been co-registered by NALC, a single transformation was applied to both image dates. Using a single image as reference ensured that all three image years were co-registered and comparable on a pixel-by-pixel basis (Yuan *et al.*, 1998). A nearest-neighbor resampling method was used to preserve the original pixel values of each image (ERDAS, 1999). The root-mean-square error (RMSE) for each image is provided in Table 3.5. The image set was visually determined to be co-registered to within +/- 1 pixel.

Table 3.5. Satellite image rectification results.

Image Date	Sensor	Rectification RMSE[*]
March 28, 1976	MSS	34.11 m
April 6, 1986	MSS	34.11 m
April 6, 1986	TM	8.68 m
April 20, 2000	ETM+	7.73 m

[*] root-mean-square error

23

Radiometric Normalization

Radiometric normalization reduces the inconsistencies in the spectral response of land-cover that are introduced by factors such as seasonal differences in sun angle, fluctuation of soil moisture content, changing atmospheric conditions, and changes in sensor calibration and performance (Eckhardt *et al.*, 1990; Jensen *et al.*, 1995; Hayes and Sader, 2001). These differences can be reduced by collecting images on or near the same day in each image year, but the sensitivity of automated change detection to changes in the spectral response of land-cover features over time requires additional processing (Eckhardt *et al.*, 1990; Hall *et al.*, 1991; Yuan *et al.*, 1998; Hayes and Sader, 2001).

There are two general approaches to radiometric normalization: (1) a true radiometric calibration, which transforms each image pixel from a brightness value to the actual ground reflectance, and (2) a relative normalization technique that uses linear regression to predict what pixel brightness values would be if they were collected at the same date and time as a reference image (Hall *et al.*, 1991; Jensen, 1996; Mas, 1999). True radiometric calibration removes the effects of atmospheric interference and noise on the measured surface reflectance. This approach requires precise atmospheric measurements at the time and place where the image was collected (Jensen, 1996). Atmospheric information is rarely available for historic imagery. Furthermore, several studies have found that the added computational complexity of a true calibration method is generally unnecessary for the purpose of

24

change detection (e.g., Jensen *et al.*, 1995; Mas, 1999). My study therefore uses a relative normalization technique.

I selected April 6, 1986 as the reference for the radiometric normalization because I had both MSS and TM images for that date. The 1976 MSS image was corrected using the 1986 MSS image as reference, and the 2000 ETM+ image was corrected using the 1986 TM image as reference. Normalization targets—constant reflectors representing the dark and bright extremes of the distribution of brightness values for each of the images—were identified using the criteria described by Eckhardt *et al.* (1990). The criteria are: (1) targets should be selected from relatively flat areas, (2) targets should contain a limited amount of vegetated land-cover to reduce the influence of environmental stress and plant phenology on spectral response, (3) targets should appear visually consistent over time, and (4) the targets should be approximately the same elevation as the rest of the scene. The diverse topography of the study area made the latter criteria impractical. All targets were therefore selected at roughly the same elevation, and it was assumed that the atmospheric interference was relatively consistent.

I visually selected normalization targets from the dark (i.e., lakes) and bright (i.e., unvegetated cropland) areas of the 1986 reference images that appeared to represent consistent land-cover features in the 1976 and 2000 subject images. The average brightness value for each target was compared to the distribution of brightness values in each band of all four images to ensure that the targets represented the extremes of

the image histogram. Targets were selected only in areas containing relatively low brightness value variance to maximize target homogeneity (Hayes and Sader, 2001).

I calculated the corrected brightness values (Y) for the subject images (2000 and 1976) from the original brightness values (S) for each subject image band (i) using the linear regression equation:

$$Y_i = m_i S_i + b_i \qquad (2)$$

The slope (m) and intercept (b) coefficients for each band are derived from the following "rectification transform" equation (Hall *et al.*, 1991):

$$m_i = \frac{Br_i - Dr_i}{Bs_i - Ds_i} \quad \text{and} \quad b_i = \frac{Dr_i Bs_i - Ds_i Br_i}{Bs_i - Ds_i} \qquad (3)$$

where Br_i is the mean brightness value for bright targets of the reference image band i, Dr_i is the mean brightness value for dark targets of the reference image, Bs_i is the mean brightness value for the bright targets of the subject image, and Ds_i is the mean brightness value for the dark targets of the subject image.

I calculated mean values for the bright and dark targets of each subject image before and after the radiometric normalization (Table 3.6). The post-normalization images appear more spectrally similar to the 1986 reference images. Significant changes in pixel brightness values between the image dates are therefore more likely to reflect a difference in surface cover. These changes in pixel brightness can be illustrated visually by replacing a portion of the subject image, both before and after normalization, with the reference image and comparing the difference in color

26

Table 3.6. 2000 ETM+ and 1976 MSS normalization target brightness value statistics before and after radiometric normalization.

	Band 1	Band 2	Band 3	Band 4	Band 5	Band 7
1986 REFERENCE TM IMAGE:						
Bright Targets	134.73	72.60	102.08	113.71	190.52	97.37
Dark Targets	74.65	29.01	24.20	9.63	5.26	2.13
2000 ETM+ IMAGE:						
Before Normalization						
Bright Targets	118.43	119.74	152.69	106.03	204.59	149.35
Dark Targets	68.88	52.24	47.37	22.28	15.48	13.10
After Normalization						
Bright Targets	134.29	72.15	101.68	113.15	189.84	96.91
Dark Targets	74.19	28.48	23.68	9.20	4.48	1.75

	Band 1	Band 2	Band 3	Band 4
1986 REFERENCE MSS IMAGE:				
Bright Targets	47.70	63.74	80.22	76.52
Dark Targets	16.44	12.56	6.69	3.75
1976 MSS IMAGE:				
Before Normalization				
Bright Targets	46.34	68.28	74.97	65.59
Dark Targets	9.31	7.56	3.56	1.00
After Normalization				
Bright Targets	47.21	63.21	79.97	75.93
Dark Targets	16.31	12.00	6.56	3.00

between the two (Figure 3.5). The combined image uses a single "lookup" table to convert the range of image brightness values into the maximum range of the display device, such as a printer or monitor. Differences between the brightness values of the original image pixels and those replaced with the subject image pixels are therefore

27
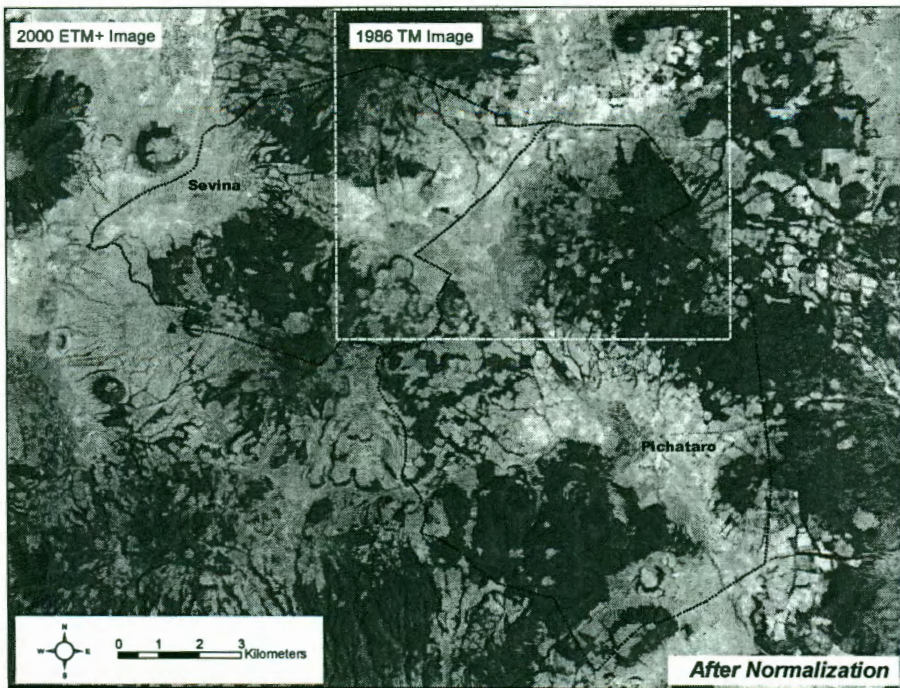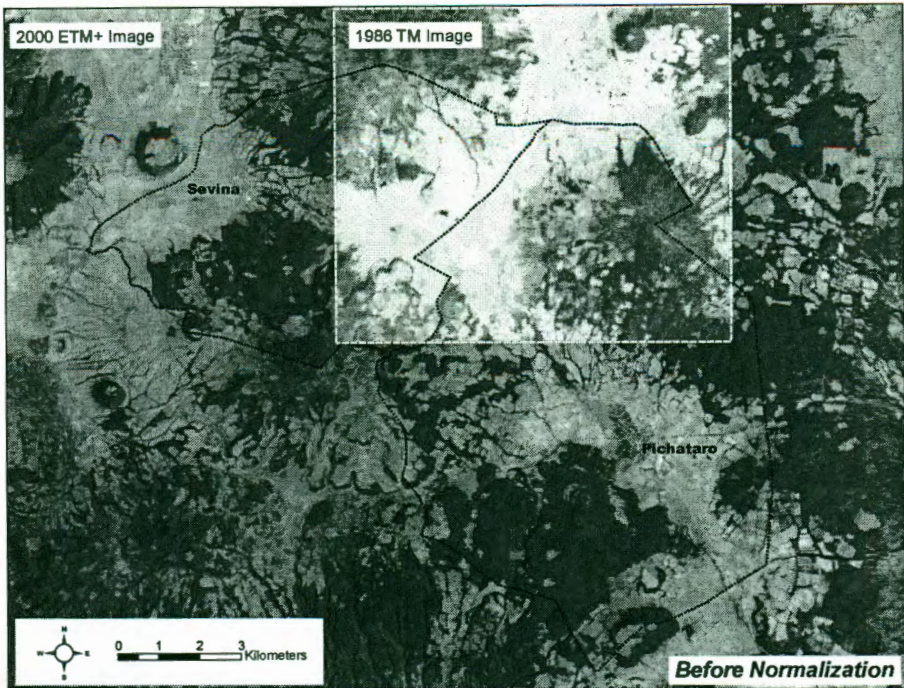
Figure 3.5. 2000 image before and after radiometric normalization. Area within white box is the 1986 reference image displayed using the same lookup table.

highlighted. The more consistent brightness of the normalized image indicates that the pixel brightness values have a more similar statistical distribution than in the non-normalized image, and can therefore be directly compared.

Topographic Normalization

Topographic normalization is the process of systematically removing the influence of relief on the spectral response of surface features. A significant limitation of using remotely sensed data in mountainous terrain is the influence of topography on the measured reflectance of surface features (Smith *et al.*, 1980; Leprieur *et al.*, 1988). In flat terrain, the near-zenith position of the satellite allows for a relatively constant sensor and illumination angle. However, in areas of high relief, illumination angles and reflection geometry vary across the image, strongly influencing the overall variability of brightness values (Smith *et al.*, 1980; Colby, 1991). This topographic effect—visually apparent in most satellite images as relief—results in areas of similar cover type exhibiting a significantly different spectral response (Civco, 1989; Colby and Keating, 1998). Because topography accounts for a large percentage of the spectral variability observed in satellite imagery, the ability to delineate between different types of land-cover is impaired, and classification results are less accurate (Walsh, 1987; Colby and Keating, 1998; Hale and Rock, 2003). I therefore applied topographic normalization to the 2000 ETM+ image to ensure the highest possible accuracy for subsequent land-cover classification.

Two trigonometric methods have been widely used to correct for topographic effects. The Lambertian model assumes that surface features are diffuse reflectors, meaning they reflect incoming solar radiation equally in all directions. Diffuse surfaces are equally bright regardless of the observation angle (Campbell, 1996). The variations in surface brightness are the result of differences in the angle of incoming solar radiation with respect to the surface, defined as the incidence angle (Colby and Keating, 1998; ERDAS, 1999). While relatively simple to apply, this method tends to overcompensate for the topographic effect, and has proven effective only for a very limited range of surface conditions (Smith *et al.*, 1980; Civco, 1989; Colby and Keating, 1998).

Several researchers have shown that the amount of reflected light is also influenced by sensor and surface geometry (e.g., the shape and orientation of plant leaves), thus departing from the Lambertian assumption (Smith *et al.*, 1980; Leprieur *et al.*, 1988; Colby and Keating, 1998; Campbell, 1996). The non-Lambertian model assumes that surface features do not reflect incoming radiation equally in all directions, but rather that the reflection is a result of the bi-directional reflection distribution function (BRDF) of illuminated phenomena as described by the Minneart constant, k (Minneart, 1941; Smith *et al.*, 1980; Campbell, 1996). The BDRF is a mathematical description of surface reflection with respect to the varying angles of illumination and observation. It is bi-directional in that it accounts for both of these angles. This method has proven more effective in representing the complex optical behavior of most surfaces (Smith *et al.*, 1980; Colby, 1991). In addition, the use of a

30
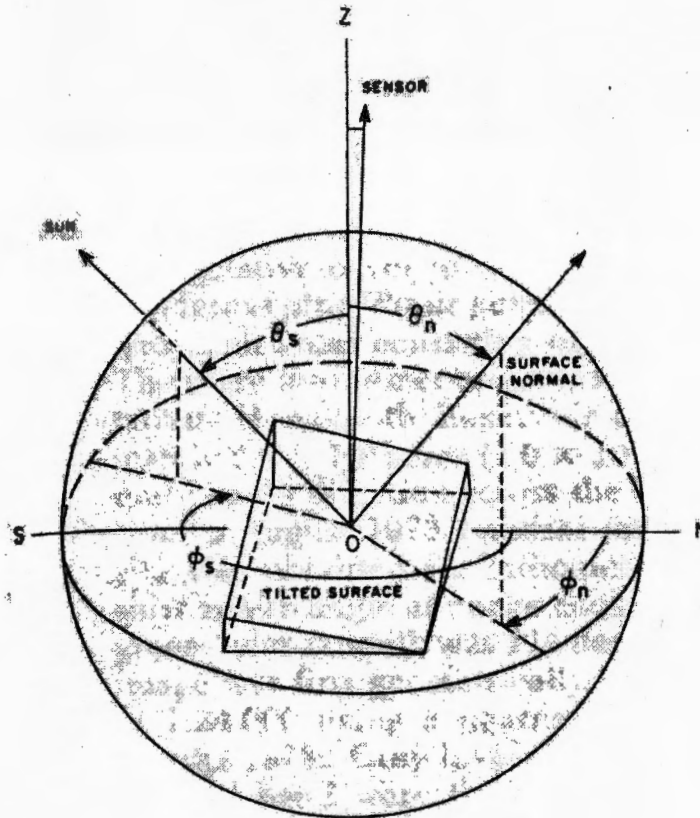
Figure 3.6. Geometric relationships between the sun, satellite sensor, and surface (adapted from Smith *et al.*, 1980), where θ_s is the solar zenith angle, θ_n is the surface normal zenith angle (which is equal to the surface slope angle), Φ_s is the solar azimuth, Φ_n is the surface azimuth (or aspect), and Z is the zenith. North (N) and South (S) are also referenced for clarity. The surface normal is perpendicular to the surface.

non-Lambertian normalization method improves land-cover classification accuracy in areas of high topographic relief (Colby and Keating, 1998; Hale and Rock, 2003).

The non-Lambertian method is based on the geometric relationships between the satellite sensor, sun, and surface (Figure 3.6). It uses the cosine of the incidence angle and the angle of reflection, or exitance angle, to normalize the image brightness based

31

on the BRDF. This approach describes satellite image pixel radiance (the measured brightness of surface features) as a function of the sun-sensor-surface geometry (Smith *et al.*, 1980):

$$L(\lambda, e) = L_n \cos^{k\lambda} i \, \cos^{k\lambda - 1} e \qquad (4)$$

where L is the pixel radiance, λ is the wavelength, e is the exitance angle, k is the Minneart constant, i is the incidence angle, and L_n is the normalized radiance that would occur when $i = e = 0°$ (i.e., both the sensor and the sun were at zenith above a flat surface).

Given the near-zenith position of the satellite, the cosine of the incidence (i) and exitance (e) angles can be determined using (Smith *et al.*, 1980; Colby, 1991):

$$\cos i = \cos \theta_s \cos \theta_n + \sin \theta_s \sin \theta_n \cos(\Phi_s - \Phi_n) \qquad (5)$$

and

$$\cos e = \cos \theta_n \qquad (6)$$

I calculated the slope (θ_n) and aspect (Φ_n) of each 30 m pixel in the study area in ERDAS Imagine using the DEM. Solar azimuth (Φ_s) and elevation at the time of collection are included in the Landsat image metadata. The solar elevation was subtracted from 90° to get the solar zenith angle (θ_s). All slope and azimuth information was converted from degrees to radians (1 radian = 180/π degrees) for
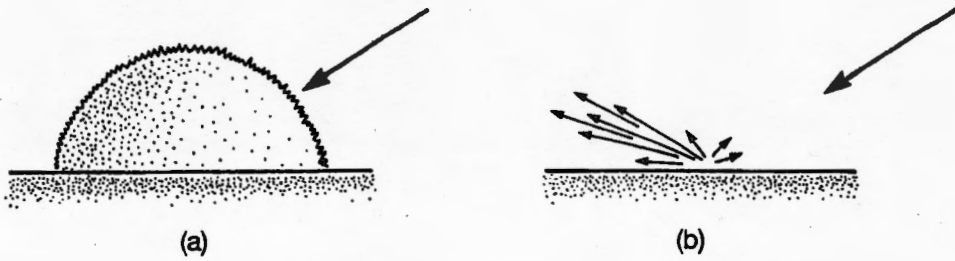
Figure 3.7. Types of surface reflection (adapted from Campbell, 1996). Diffuse reflection (a) occurs when surfaces scatter incoming solar radiation equally in all directions ($k=1$). Specular reflection (b) occurs when surfaces tend to scatter radiation in a single direction ($k \neq 1$).

performing calculations. I developed an ERDAS model to calculate cos i and cos e for each pixel using equations (5) and (6).

The Minneart constant k is considered an abstraction of the surface feature geometry, or "roughness" (Smith *et al.*, 1980; Colby, 1991). When $k = 1$, the surface behaves in a Lambertian (diffuse) manner, and the constant is irrelevant (Figure 3.7a). Values of k less than or greater than 1 indicate combinations of diffuse and specular scattering (Smith *et al.*, 1980). Specular scattering occurs when a surface scatters most or all incoming radiation in a single direction, like a mirror (Campbell, 1996) (Figure 3.7b).

In studies by Smith *et al.* (1980) and Colby (1991), the Minneart constant was derived by linearizing equation (4) and then obtaining the regression value for k:

$$L \cos e = L_n \cos^k i \ \cos^k e \qquad (7)$$

and:

$$\log (L \cos e) = \log L_n + k \log (\cos i \ \cos e) \qquad (8)$$

33

which assumes the form of the standard linear regression equation $y = kx + b$, where $\log (L \cos e)$ is the dependent variable y, $\log L_n$ is the y intercept of the regression line b, and $\log (\cos i \, \cos e)$ is the independent variable x. The Minneart constant k is the slope (Colby *et al.*, 1998).

Because the Minneart constant represents surface roughness, it varies among different land-cover types. Ideally, it would be derived from sample pixels representing a single surface feature and applied only to pixels in that land-cover class (Colby *et al.*, 1998; ERDAS, 1999; Hale and Rock, 2003). However, this requires *a priori* knowledge of the region. Given that the extent of the various surface cover classes is typically unknown prior to image classification, the constant k is usually generalized from a topographically-diverse sample of the dominant land-cover and applied to the entire image (Colby *et al.*, 1998; Hale and Rock, 2003).

For the 2000 ETM+ image, I identified four sites containing relatively uniform forest stands using the information collected in the field. These sample sites included a variety of surface orientations to ensure a range of incidence and exitance angles (Colby *et al.*, 1998). The sample areas were compared with the 1990 aerial photos and the 2000 ETM+ panchromatic image, and any sites that did not appear forested in both years were eliminated. This increased the likelihood that these areas represented well-established stands. A model was developed in ERDAS to solve regression equation (8) for k for each of the 2000 image bands (Table 3.7).

Table 3.7. Minneart constants (k) for the 2000 ETM+ image.

Band 1	0.274
Band 2	0.285
Band 3	0.251
Band 4	0.550
Band 5	0.406
Band 7	0.342

I calculated the normalized radiance using a backward radiance correction transformation (BRCT) regression equation (Smith *et al.*, 1980; Colby, 1991):

$$L_n = \frac{L \cos e}{\cos^k i \, \cos^k e} \tag{9}$$

A model based on equation (9) was created in ERDAS to create the normalized image using the original 2000 ETM+ image, the cosine images created using equations (5) and (6), and the Minneart constants from Table 3.7. The impression of relief is visually reduced in the normalized image (Figure 3.8).

I did not apply topographic correction to the 1976 and 1986 images because they were not being used for supervised image classification. I used the 1976 and 1986 images as inputs into an automated change detection process, where topographic effects are minimized by using a ratio of image bands (Hayes and Sader, 2001).

35

(a)
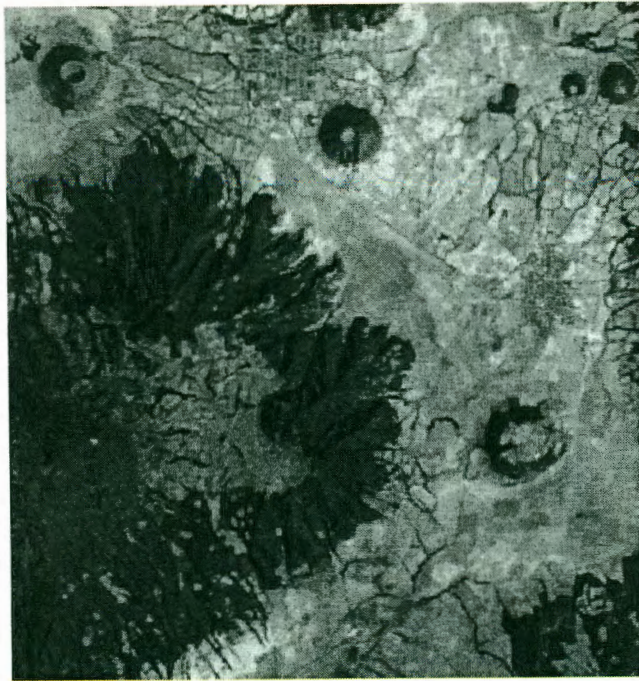
(b)
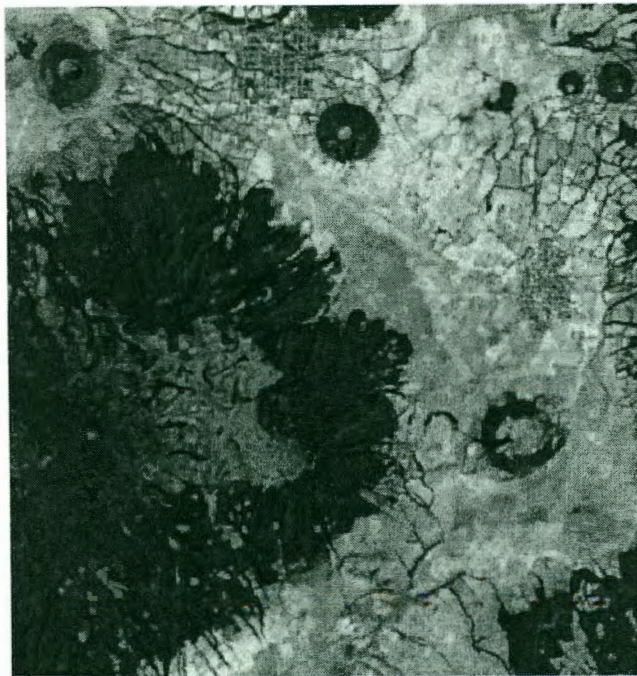
Figure 3.8. 2000 ETM+ image before (a) and after (b) topographic normalization.

Land-cover Classification

Land-cover classification is the process of assigning satellite image pixels to a particular land-cover class based on the pixel's spectral response, defined as the measured brightness of a pixel across the image bands. There are two general approaches to image classification—unsupervised and supervised. Unsupervised classification identifies groups of pixels that exhibit a similar spectral response. These spectral classes are then assigned to land-cover classes by the analyst. However, in many cases the spectral classes do not correspond well with the desired land-cover classes (Campbell, 1996; Kelly *et al.*, 2004). The spectral and land-cover classes may overlap, but there is rarely a one-to-one relationship.

Supervised classification uses image pixels representing regions of known, homogenous surface composition to classify unknown pixels. The collection of known pixels is referred to as the training area. The underlying assumption is that spectral response of a particular land-cover will be relatively consistent throughout the image. The main advantage of supervised classification is that it results in a usable map of land-cover based on classes defined by the analyst (Kelly *et al.*, 2004). I use a supervised technique in my study for this reason.

I identified 35 training areas in the 2000 ETM+ image using the GPS-delineated stand areas and land-cover features. I used a seeding technique to "grow" training areas outward from a single pixel selected in the approximate center of the GPS-delineated sample areas. Contiguous pixels with brightness values within +/-10 brightness numbers of the seed pixel in all of the visible and near-infrared bands were
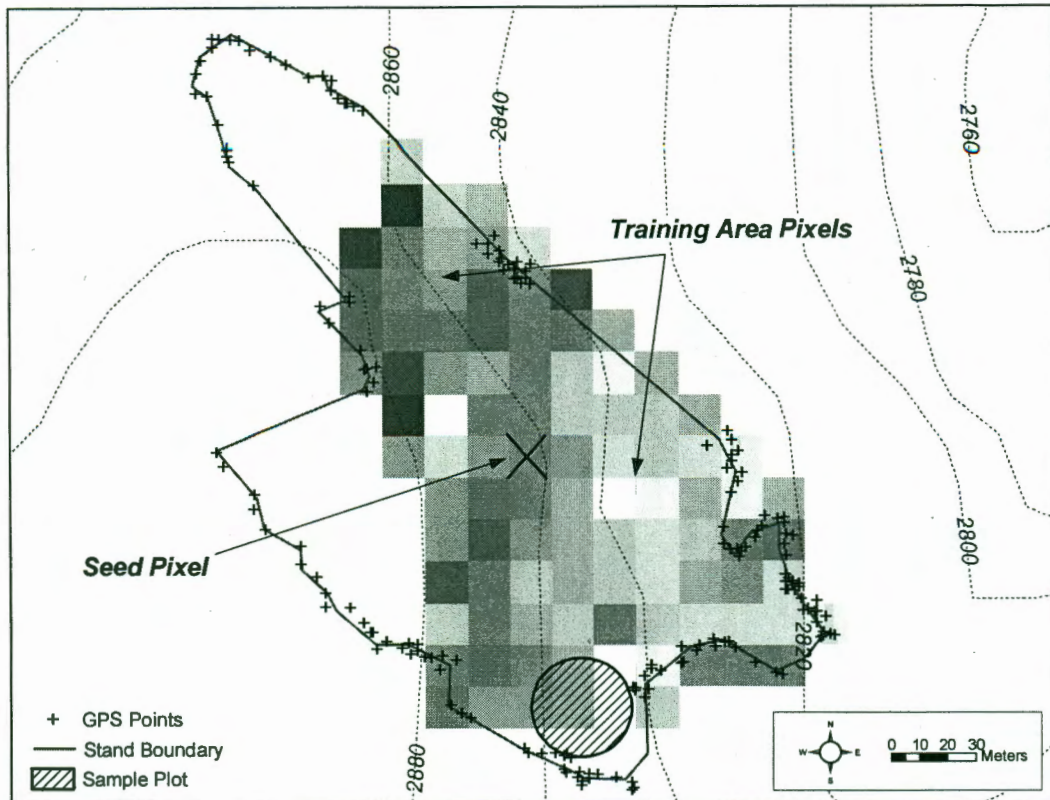
Figure 3.9. Training area for the stand surrounding sample plot 'South Sevina #4.' The different shades of gray represent different pixel brightness values.

added to the training area collection. The seeding process continued until no more

contiguous pixels satisfying this criteria were found (Figure 3.9).

There are several reasons I used a seeding technique to define training areas rather

than using the GPS-delineated sample areas directly: (1) it ensured that pixels within

the training area had a limited range of brightness values and were therefore more

likely to represent a single land-cover feature, (2) it compensated for any differences

in vegetation between the April 2000 date of the satellite image and the August 2000

date of the field data collection, (3) it reduced the likelihood of errors resulting from differences in the registration between the image and the GPS data, and (4) because the seeding process was not constrained to the GPS-delineated sample area, it allowed for larger training areas where the GPS sample captured only a portion of a forest stand or other land-cover.

I grouped the training areas into general land-cover classes using the plot summary data. Forested training areas were classified as pine, mixed pine (pine dominant), mixed oak (oak dominant), and mixed fir (fir dominant). Non-forested training areas were classified as scrub/shrub, agriculture (maize), grassland, and non-vegetated (minimal vegetation and bare earth). I inspected the histogram of brightness values for each training area for multi-modality, or multiple peaks in the distribution. A multi-modal distribution indicates the presence of more than one land-cover feature in the training area (Jensen, 1996; Mas and Ramirez, 1996; ERDAS, 1999). Areas exhibiting multi-modal pixel value distributions were removed from the training set. A total of 32 training areas were considered acceptable for image classification (Table 3.8).

Table 3.8. Summary of 2000 ETM+ image training areas.

Land-cover	Number of Training Areas	Number of pixels	Total Area (ha)
Pine Forest	4	136	12.24
Mixed Pine Forest	11	357	32.13
Mixed Oak Forest	1	23	2.07
Mixed Fir Forest	2	68	6.12
Grassland	2	99	8.91
Scrub/Shrub	2	32	2.88
Agriculture	2	236	21.24
Unvegetated	8	1109	99.81
Column Total	32	2060	185.40
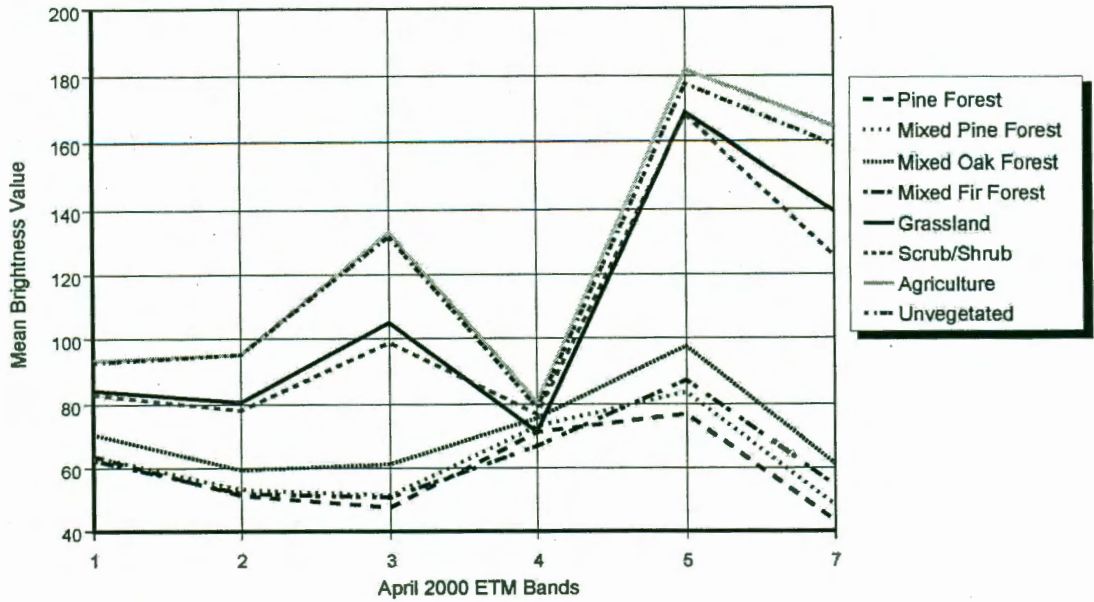
Figure 3.10. 2000 ETM+ image spectral signatures for all land-cover classes.

I examined the spectral signature of each land-cover class relative to the other classes (Figure 3.10). The spectral signature represents the mean training area brightness value for each class in the 6 ETM+ image bands. Classes with similar spectral signatures are difficult to differentiate in the image and have a negative effect on the classification accuracy (Jensen, 1996). I also performed a contingency analysis of the training areas to examine the overlap in the range of brightness values between the land-cover classes. Contingency analysis produces a matrix showing the percentage of pixels that are classified correctly in a preliminary image classification of *only* the training areas (Table 3.9). It assumes that most of the training area pixels should be assigned to their respective land-cover class. If a significant percentage of

40

training pixels are classified as another land-cover, it indicates that the spectral signatures are not distinct enough to produce an accurate classification of the entire image (ERDAS, 1999).

Table 3.9. Contingency matrix for all land-cover types (numbers represent training area pixels).

				Actual Land-cover				
Classified Land-cover	Pine	Mixed Pine	Mixed Oak	Mixed Fir	Grass	Scrub	Agricult	UnVeg
Pine	101	96	1	2	0	0	0	0
Mixed Pine	24	213	3	2	0	0	0	0
Mixed Oak	4	23	19	0	0	0	0	0
Mixed Fir	7	25	0	64	0	0	0	0
Grass	0	0	0	0	90	1	9	55
Scrub	0	0	0	0	2	31	0	0
Agricult.	0	0	0	0	2	0	213	57
UnVeg	0	0	0	0	5	0	14	997
Column Total	136	357	23	68	99	32	236	1109
% Correct	74.3%	59.7%	82.6%	94.1%	90.9%	96.9%	90.3%	89.9%

My signature evaluation and contingency matrix revealed that the four forested classes were too spectrally similar to be delineated effectively. The mixed oak (23 pixels) and mixed fir (68 pixels) training areas are most likely too small to distinguish them from the pine and mixed pine classes. This is not surprising given the relatively limited distribution of these stand types in the Meseta (Watts and Bradbury, 1982; Perry, 1991). The mixed stands were also difficult to consistently sample because of inherent differences in composition. The mixed pine stands contained different percentages of fir and oak, for example. The classification therefore tends to confuse the pine, mixed pine, and mixed oak classes. Similar classification confusion occurred
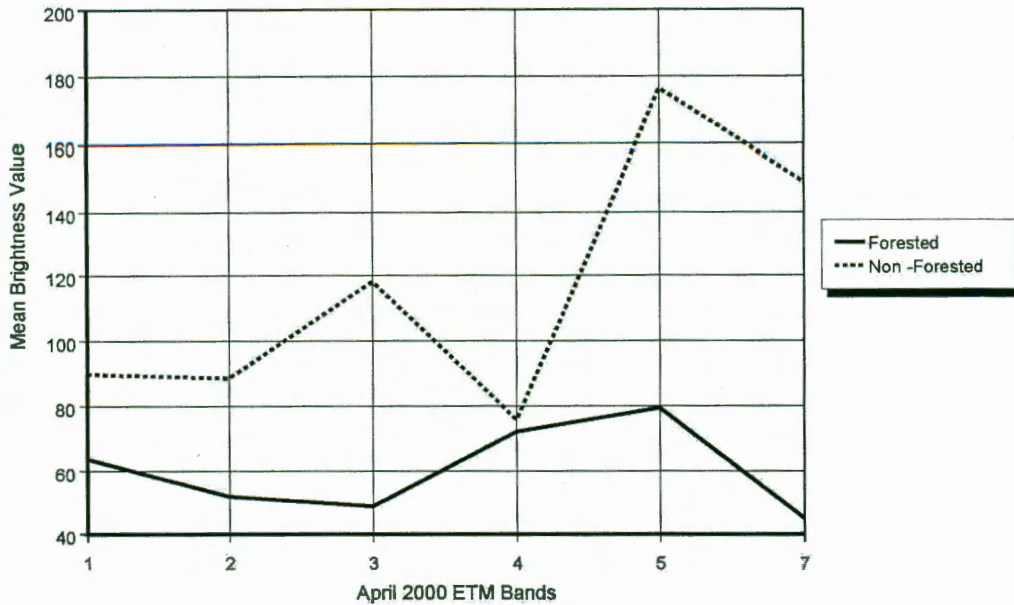
Figure 3.11. 2000 ETM+ image spectral signatures for aggregated land-cover classes.

within the non-forested classes.

Failing attempts to create spectrally-distinct signatures for the individual land-cover classes, I aggregated the training areas into two basic land-cover classes—forested and non-forested (Mertins and Lambin, 2000). The spectral signatures of the two aggregated classes were unique (Figure 3.11), and the contingency analysis showed a clear differentiation between the two land-cover classes (Table 3.10).

Table 3.10. Contingency matrix for aggregated land-cover types (numbers represent training area pixels).

	Actual Land-cover	
	Forested	Non-Forested
Forested	517	0
Non-Forested	0	3016
Column Total	517	3016
% Correct	100%	100%

I used a maximum likelihood method to classify the image. Maximum likelihood classifiers use the training area brightness value statistics to generate a covariance matrix between the forest and non-forest classes, which is then used to estimate the probability that an image pixel belongs to a given class (Campbell, 1996; ERDAS, 1999). This method usually produces the most accurate classification result when using good-quality training data (Campbell, 1996; Jensen, 1996; ERDAS, 1999).

To assess the accuracy of the classification, I created a set of reference points using ERDAS Imagine. I randomly selected thirty points from both the forested and non-forested categories using a 3 by 3 roving window, where all nine pixels in the window belonged to the same class to avoid edge effects that complicate visual interpretation (Hayes and Sader, 2001). Each point was visually classified as forest or non-forest using the 2000 ETM+ image as reference. Visual classification of satellite-imagery reference points has been shown to be an effective assessment technique comparable to more traditional methods using aerial photo interpretation and field sampling (Mas and Ramirez, 1996; Cohen *et al.*, 1998).

Automated Change Detection

Change detection identifies the differences in land-cover between remotely-sensed images covering two or more time periods. Four aspects of change detection are considered important when managing natural resources or measuring anthropogenic disturbance (Macleod and Congalton, 1998): (1) detecting changes that have occurred, (2) identifying the nature of the change, (3) measuring the area and extent of the change, and (4) assessing the spatial pattern of the change.

Change detection methods generally fall into two categories—classification-based and spectrally-based. The most widely used classification-based method is post-classification comparison, where land-cover change is derived from the comparison of two independently classified image dates. Post-classification comparison is often used because it is easy to perform and interpret (Jensen, 1996). All the images in a time series are simply compared on a pixel-by-pixel basis. However, this method is highly dependent upon the classification accuracy of each image in the series. The accuracy of a post-classification comparison can be estimated by multiplying the overall accuracy of the input images (Yuan *et al.*, 1998). If, for example, one classified image has an accuracy of 82% and the other classified image has an accuracy of 80%, the resulting post-classification comparison would have an accuracy of only 65.6%. In most circumstances, this would not be considered an acceptable accuracy for land-cover classification (Campbell, 1996; Jensen, 1996). It is therefore important that all input land-cover classifications are as accurate as possible. Unfortunately, it is difficult

to generate a highly accurate historic classification in areas where little or no historic reference data exist.

Spectrally-based methods are generally preferred for change detection because they tend to produce a higher accuracy result than classification-based methods (Jensen, 1996; Yuan *et al.*, 1998). One of the most frequently used methods is image differencing. A variety of image differencing techniques are in use, though all involve the same basic process—one image date is subtracted from another image date to highlight areas where there has been a significant change in pixel brightness value (Yuan *et al.*, 1998, Hayes and Sader, 2001). All input images must be co-registered and radiometrically normalized to effectively use an image differencing technique. A difference threshold must also be established to differentiate areas of actual change from those that result from the natural variations in land-cover and minor radiometric differences between the input images (Fung and LeDrew, 1988; Hayes and Sader, 2001).

Using the original image bands for image differencing means that each band must be processed separately, making it difficult to interpret the collective results. Consequently, band ratios or vegetation indices are often used to identify changes in a specific land-cover feature (Lyon *et al.*, 1998; Hayes and Sader, 2001). The normalized difference vegetation index (NDVI) (the normalized difference between brightness values from the red and near-infrared image bands) has been widely used as a measure of both the presence and health of vegetation including coniferous and deciduous forests (Tucker, 1979, Running *et al.*, 1986; Jensen, 1996; Hayes and Sader,

45

2001). The NDVI is based upon findings that the chlorophyll in plant leaves strongly absorbs visible light (from 0.4 to 0.7 μm), while the cell structure of the leaves strongly reflects near-infrared light (from 0.7 to 1.1 μm) (Tucker, 1979).

The NDVI for a given pixel p is calculated as (Mas, 1999):

$$NDVI_p = \frac{NIR_p - R_p}{NIR_p + R_p}$$
(10)

where *NIR* is the near-infrared response of pixel p and *R* is the visible red response. Lyon *et al.* (1998) tested several vegetation indices for their applicability to image differencing and found NDVI to be the most effective for identifying vegetation change, particularly areas of deforestation.

NDVI Image Differencing

I generated a NDVI image for each date of imagery using the following equations (ERDAS, 1999):

MSS images: $$NDVI = \frac{[MSS4 - MSS2]}{[MSS4 + MSS2]}$$
(11)

TM images: $$NDVI = \frac{[TM4 - TM3]}{[TM4 + TM3]}$$
(12)

Because both a MSS and TM image was available for April 1986, a NDVI image was generated for each sensor. This allowed for a direct comparison between the 1976 and

1986 MSS and 1986 and 2000 TM/ETM+ NDVI images by restricting all comparisons to a single sensor.

I created the NDVI-difference images by subtracting the 1976 and 1986 image dates from the 1986 and 2000 image dates, respectively (Hayes and Sader, 2001):

MSS images: DIFF[1976 to 1986] = NDVI[1986] − NDVI[1976]   (13)

TM images: DIFF[1986 to 2000] = NDVI[2000] − NDVI[1986]   (14)

A small area of cloud cover present in the 1986 image was digitized and removed from all image dates prior to differencing to eliminate this area from further analysis.

Kappa Thresholding

To create a classified forest change image, thresholds must be established to separate areas of change from areas of no change in the NDVI-difference images. One common approach is to iteratively test thresholds by adding and subtracting multiples of the standard deviation of the NDVI-difference image from its mean (Jensen, 1996; Hayes and Sader, 2001). The following formulas illustrate:

$$T_l = \mu_d - (\sigma_d N)$$ (15)

and

$$T_u = \mu_d + (\sigma_d N)$$ (16)

where T_l is the lower threshold, T_u is the upper threshold, μ_d is the mean of NDVI-difference image d, σ_d is the standard deviation of NDVI-difference image d, and N is

the standard deviation multiplier. Fung and Ledrew (1988) found that the standard deviation multiplier N that produced the best combination of accuracy and efficiency was 0.2.

I calculated the mean difference and standard deviation for each of the two NDVI-difference images (Table 3.11). The N value was set at 0.2 for the first thresholding iteration. Pixels with a NDVI-difference value of less than the lower threshold (T_l) were classified as forest clearing; all other pixels were classified as not cleared. In an independent process, pixels with a value of greater than the upper threshold (T_u) were classified as areas of forest regrowth; all other pixels were classified as not regrown. For each subsequent iteration, the N value was increased by a value of 0.2 until N equaled 2.

Table 3.11. NDVI difference image statistics.

Image Years	Mean Difference	Standard Deviation
1986 to 2000	0.037	0.124
1976 to 1986	-0.024	0.066

Two change classification images were therefore produced at each iteration for both sets of image dates—a forest clearing/no clearing classification and a forest regrowth/no regrowth classification. The forest clearing and forest regrowth change categories were therefore maximized independently for each tail of the NDVI-difference image histogram (Hayes and Sader, 2001) (Figure 3.12). Independent

(a) "Clearing" threshold

$$T_l = \mu_d - (\sigma_d N) \qquad \mu_d$$

(b) "Regrowth" threshold

$$\mu_d \qquad T_u = \mu_d + (\sigma_d N)$$
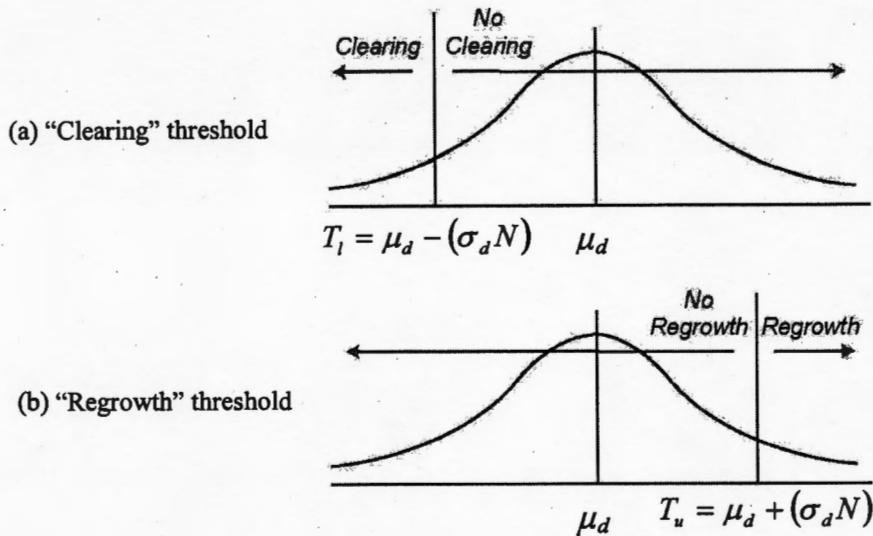
Figure 3.12. Illustration of the independent thresholding of the forest clearing (a) and forest regrowth (b) change categories, where μ_d is the mean of the NDVI-difference image d, σ is the standard deviation of NDVI-difference image, and N is the standard deviation multiplier.

processing was necessary given the possibility that the change in NDVI resulting from forest clearing was not proportional to the change resulting from forest regrowth (e.g., a decrease in NDVI of 1.5 standard deviations may indicate forest clearing, while an increase of only 1 standard deviation may indicate forest regrowth).

Fung and LeDrew (1988) demonstrated that this type of change image thresholding is most effective if the Kappa coefficient is used to assess of the accuracy of the classifications produced at each iteration. The Kappa coefficient $\hat{K}$ is computed as (Congalton and Green, 1999):

$$\hat{K} = \frac{M \sum_{i=j=1}^{r} n_{ij} - \sum_{i=j=1}^{r} n_i n_j}{M^2 - \sum_{i=j=1}^{r} n_i n_j} \qquad (17)$$

where r is the number of rows in the accuracy assessment error matrix, n_{ij} is the number of observations in row i and column j, n_i is the total number of observations for row i, n_j is the total number of observations for column j, and M is the total number of observations in the matrix.

The overall classification accuracy is the total number of correctly classified samples divided by the total number of samples; it measures the accuracy of the entire image without reference to the individual categories. The overall accuracy is therefore sensitive to differences in sample size and tends to be biased towards the categories with larger samples (Fung and Ledrew, 1988; ERDAS, 1999). The Kappa coefficient is not as sensitive to differences in sample sizes between categories and is therefore considered a more reliable measure of accuracy (Congalton and Green, 1999). Kappa measures the actual agreement less the chance agreement in an error matrix by considering both errors of commission and omission (Rosenfield and Fitzpatrick-Lins, 1986; Jensen, 1996; Congalton and Green, 1999). In a simple forest and non-forest classification, an error of omission occurs within the forest class when forested pixels are assigned to the non-forest class, thus omitting those pixels from their true class. The measure of the error of omission is commonly referred to as the producer's accuracy (Congalton and Green, 1999). Conversely, an error of commission occurs within the forest class when non-forested pixels are assigned to the forest class; the error has been committed to the forest class. The measure of the error of commission is referred to as the user's accuracy (Congalton and Green, 1999). Note that all errors

50

of omission in one class will be recorded as errors of commission in another class (Jensen, 1996; Congalton and Green, 1999). By considering errors of both commission and omission, the Kappa coefficient expresses the reduction in error generated by the classification in comparison with a completely random process (Congalton and Green, 1999; ERDAS, 1999). A Kappa of 0.78, for example, indicates that 78% of the errors that would occur in a completely random classification are being avoided. Landis and Koch (1977) characterized three general groupings of Kappa coefficients: values greater than 0.80 represent strong agreement; values between 0.40 and 0.80 represent moderate agreement; and values below 0.40 represent poor agreement.

I created error matrices for the Kappa thresholding using a set of randomly selected reference points. Using a process similar to that reported by Hayes and Sader (2001), I scaled each NDVI-difference image into an 8-bit image with pixel values from 0 to 255. The 8-bit image was separated into 16 individual classes; values from 1 to 16 became one class, 17 to 32 another, and so forth. I used a stratified sampling technique to systematically select a minimum number of random reference points from each of the 16 classes. To avoid edge pixels near the boundary of two or more classes, points were selected using a 3 by 3 roving window where all 9 pixels in the window belonged to the same class. A minimum of 5 points were selected from each class. This guaranteed a diverse sample of NDVI-difference values that were well distributed throughout the image histogram.

I created a total of 125 reference points for the 1986 to 2000 change classification images. Each of the random points was classified as forest clearing, forest regrowth, or

no change using visual interpretation of the 1986 TM and 2000 ETM+ images. A total of 164 points were classified for the 1976 to 1986 NDVI-difference image using the 1976 MSS and 1986 MSS/TM images as reference.

I generated an error matrix at each thresholding iteration by comparing the clearing and regrowth change classifications with the reference points (Table 3.12). The error matrix Kappa coefficient was calculated at each iteration and plotted to identify the optimum threshold for each category (Figure 3.13). The lower Kappa coefficients for the 1976 to 1986 difference image result from the decreased spatial and spectral resolution of the MSS sensor. Less clearing and regrowth also occurred between these two image dates in comparison with the 1986 to 2000 image period. Nonetheless, these values are within the acceptable range of accuracy for this type of imagery and are similar to the results of other studies relying on MSS data (Landis and Koch, 1977; Congalton and Green, 1999).

Table 3.12. Example of an error matrix from the first iteration of the 1986 to 2000 forest clearing change image change thresholding ($N = 0.2$).

Cleared versus Not Cleared			
	Reference Data		
Classified Data	Cleared	Not Cleared	Row Totals
Cleared	32	23	55
Not Cleared	1	69	70
Column Totals	33	92	125

	Producer's Accuracy	User's Accuracy
Cleared	97.0%	58.2%
Not Cleared	75.0%	98.6%

Overall Accuracy:	80.8%	
KAPPA:	0.593	
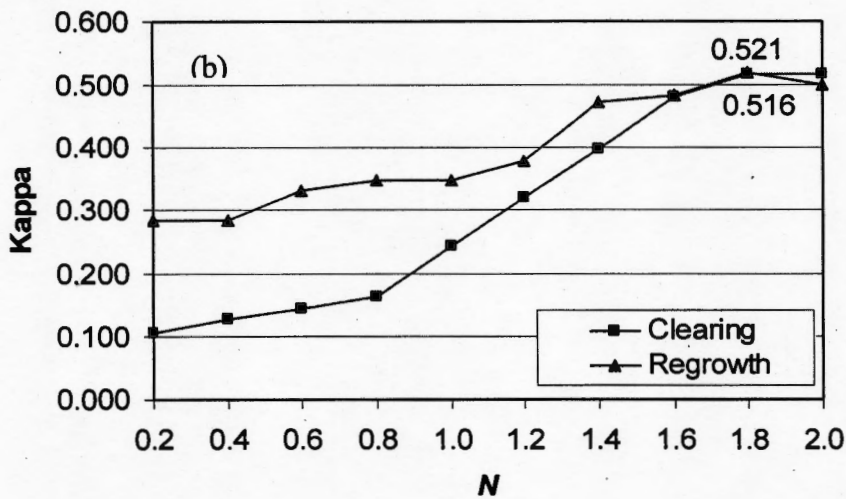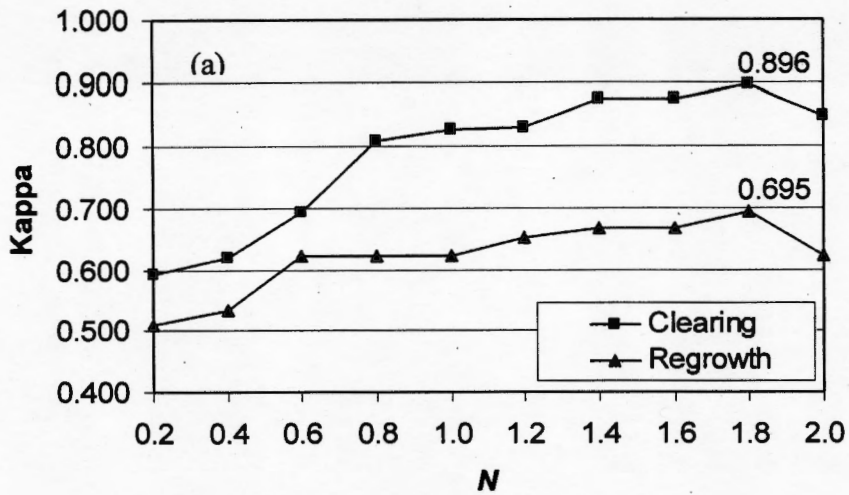
Figure 3.13. Kappa thresholding of 1986 to 2000 (a) and 1976 to 1986 (b) NDVI-difference images, where N is the NDVI-difference image standard deviation multiplier.

I used the threshold that produced the highest Kappa coefficient for change categories to produce a single, aggregated change classification for both image periods

(Table 3.13). The final change image classes are forest clearing, forest regrowth, and areas of no change (Hayes and Sader, 2001).

Table 3.13. Final Kappa-optimizing thresholds of 1986 to 2000 and 1976 to 1986 change images.

Image Years	Clearing Threshold	Clearing KAPPA	Regrowth Threshold	Regrowth KAPPA	Overall KAPPA
1986 to 2000	-0.186	0.896	0.260	0.695	0.750
1976 to 1986	-0.144	0.516	0.094	0.521	0.502

I improved the 1986 to 2000 change classification by comparing the results with the 2000 land-cover classification. The 2000 land-cover classification was based on recently collected field data and produced a map of relatively high accuracy (see Table 4.2). Therefore, I assumed that information regarding forest presence or absence contained in this image superseded any conflicting information resulting from the automated change detection process. I created a model in ERDAS Imagine to perform the comparison on a pixel-by-pixel basis. Any conflicts were resolved using a set of rules enforcing the results of the 2000 classification (Table 3.14). I also processed both the 1976 to 1986 and 1986 to 2000 change images to assign all non-contiguous groups of less than three image pixels (2700 m^2) to the no change category. This reduced the effect of any slight misregistration between the image dates and removed image "speckle" (ERDAS, 1999).

54

Table 3.14. Refinement rules for 1986 to 2000 forest change image.

2000 Supervised Classification Image	Original 1986 to 2000 Change Image	*Refined 1986 to 2000 Change Image*
Forested	Regrowth	*Regrowth*
Forested	No Change	*No Change*
Forested	Cleared	*No Change*
Non-Forested	Regrowth	*No Change*
Non-Forested	No Change	*No Change*
Non-Forested	Cleared	*Cleared*

Temporal Classification of Forest Extent

A significant limitation of most automated change detection techniques is the inability to produce a land-cover map for each image date (Pilon *et al.*, 1988; Yuan *et al.*, 1998). Change detection methods use a comparative technique to identify only the areas of change between a set of image dates rather than the overall extent of a particular land-cover at a given time. My study uses a hybrid method that relies on a supervised land-cover classification of a single base year image to systematically classify all other image years using the forest change information derived from the automated change detection. This "temporal classification" technique requires only one set of training data to classify a single base image year. Other image years can be classified without specific knowledge of ground conditions at those dates (Pilon *et al.*, 1988). Temporal classification is especially useful when working with historic data, where reliable reference information is often unavailable.

Using the 2000 supervised classification as the base information and the 1986 to 2000 change classification as a reference for areas of forest clearing and regrowth

55

since 1986, I created a temporal classification of the 1986 TM image based on a set of rules for determining the forested extent (Table 3.15). I developed a model in ERDAS to do a pixel-by-pixel comparison of the two images and generate a map of total forest extent in 1986. A set of 30 random reference points was used to assess the accuracy of the classification.

Table 3.15. Rules for temporal classification of 1986 TM image.

2000 Supervised Classification Image	Refined 1986 to 2000 Change Image	1986 Temporal Classification Image
Forested	Regrowth	Non-Forested
Forested	No Change	Forested
Non-Forested	No Change	Non-Forested
Non-Forested	Cleared	Forested

I used a similar approach to map forest extent in 1976. The 1986 temporal classification of forest extent served as the base image and the 1976 to 1986 change classification image was used as a reference to identify areas of clearing and regrowth since 1976. I used the ERDAS model to classify forest extent based on a pixel-by-pixel comparison between the 1986 classification and change classification images. The accuracy assessment was performed using a set of 30 randomly generated points.

Forest Change Trajectories

Forest change trajectories represent successive transitions between forested land-cover categories over the time period being observed (Mertens and Lambin, 2000). For example, a non-forested area in the 1976 image may transition to forest in

56

the 1986 image, returning once again to non-forested in the 2000 image. This creates a shifting landscape mosaic resulting from successive transitions from non-forested to forested to non-forested. These trajectories can be mapped by comparing land-cover classifications for a series of image dates.

I created a map of forest change trajectories for the twenty-four year period between 1976 and 2000 using techniques described by Southworth *et al.* (2002). I developed a model in ERDAS to perform a pixel-by-pixel comparison of the 1976, 1986 and 2000 images of forest extent, resulting in a single change trajectory image separated into the eight forested land-cover change descriptions originally developed by Mertens and Lambin (1997, 2000) (Table 3.16). Each pixel in the study area was assigned to one of the eight land-cover trajectory categories.

Table 3.16. Forest change trajectories derived from three classified image dates (1976, 1986 and 2000).

1976 Temporally-Classified Image	1986 Temporally-Classified Image	2000 Supervised Classification Image	Land-cover Trajectory Description[1]
Forested	Forested	Forested	Stable Forest
Forested	Non-Forested	Non-Forested	Older, more permanent forest clearing
Forested	Non-Forested	Forested	Old forest clearing with regrowth
Forested	Forested	Non-Forested	Recent forest clearing
Non-Forested	Non-Forested	Non-Forested	Stable agriculture/non-forested area
Non-Forested	Forested	Non-Forested	Forest regrowth with new clearing
Non-Forested	Forested	Forested	Older, more permanent forest regrowth
Non-Forested	Non-Forested	Forested	Recent forest regrowth

[1] adapted from Mertens and Lambin (2000)

Landscape Metrics

I calculated landscape metrics for the 1976, 1986 and 2000 maps of forest extent and the forest change trajectories using Fragstats 3.3 software. Landscape metrics statistically describe differences in the spatial distribution of land-cover patches, which are defined as contiguous areas of a homogenous land-cover (Southworth *et al.*, 2002). Although many metrics are available, I used a set of 7 metrics shown to be effective and easily interpreted in studies of changes in land-cover classes (Ritters *et al.*, 1995; Frohn, 1998; Southworth et al., 2002) (Table 3.17). The indices of percentage land-cover (PLAND), largest-patch index (LPI), number of patches (NP), mean patch size (MPS), and edge density (ED) are useful for identifying the differing degree of fragmentation of land-cover classes over time. The mean shape index (MSI) provides a measure of the difference in shape complexity between classes. The mean Euclidean nearest-neighbor distance (MENN) indicates the relative level of isolation of each land-cover class (McGarigal and Marks, 1994; Southworth et al., 2002). McGarigal and Marks (1994) provide a detailed description of each metric with the formulas necessary for calculation.

Table 3.17. Summary of landscape metrics used in this study.

Metric	Description
Percentage land-cover (PLAND)	Percentage of total area occupied by each class.
Largest-patch index (LPI)	Area of the largest patch in each class (in percentage of total landscape area).
Number of patches (NP)	Total number of patches in the class.
Mean patch size (MPS)	Mean patch size for the class in hectares.
Edge density (ED)	Sum of all edge segments for the class divided by total landscape area.
Mean shape index (MSI)	Average complexity of patch shape for a class (the index is 1 when the patch is square, and increases infinitely as the patch becomes more irregular.
Mean Euclidean nearest-neighbor distance (MENN)	The mean distance in meters to the nearest neighboring patch of the same class, based on shortest edge-to-edge distance. Approaches 0 as the distance to the nearest neighbor decreases.

CHAPTER 4: RESULTS AND DISCUSSION

Forest Conditions in April 2000

Field Data Analysis

Field data illustrate a range of biophysical conditions for the respective communal

forests of Sevina and Pichátaro (Table 4.1). The forests managed by Sevina had, on

average, younger, shorter pine trees that presented a smaller DBH relative to Pichátaro

(Figure 4.1).

Table 4.1. Pichátaro and Sevina field data analysis summary (pine only; values are significantly different at $P<0.01$).

	Sevina	Pichátaro
Total number of plots sampled	10	10
Total area of plots (m^2)	7,375	9,250
Total number of trees	339	247
Mean density of trees (trees/ha)	428.05	349.19
Mean tree DBH (cm)	23.26	29.86
Mean tree age (in years)[1]	26.55	31.05
Mean tree height (m)[2]	16.50	18.74

[1] includes predicted values for tree age from linear regression analysis ($R^2 = 0.667$) based on the 104 trees cored in the field.
[2] includes predicted values for tree height from linear regression analysis ($R^2 = 0.817$) based on the 116 trees measured in the field.

The differences support the hypothesis that Sevina has more dramatically altered

its forested areas over the last several decades (Works and Hadley, 2004). The field
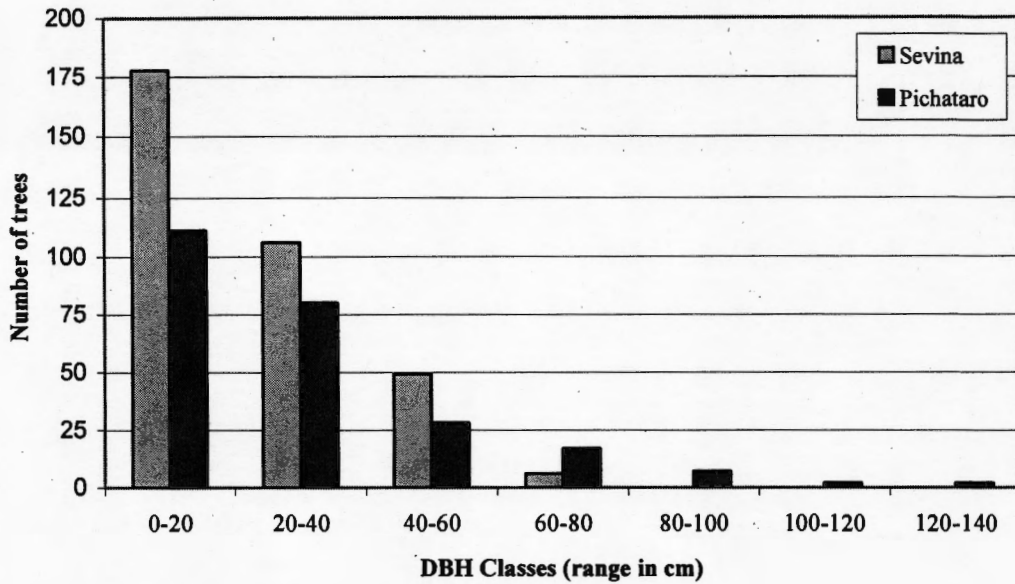
Figure 4.1. Pine DBH class distributions for Sevina and Pichátaro in 20 cm DBH classes.

data suggest that more of Sevina's large pines have been harvested, leaving younger, smaller stands in their place.

2000 Land-cover Classification Results

The result of the supervised land-cover classification is a map of total forest extent in 2000 (Figure 4.2). The accuracy assessment of the classification image indicates an overall accuracy of 93.3% with a Kappa coefficient of agreement of 0.867 (Table 4.2). This suggests that there is a relatively strong agreement between the reference data and the classified image.
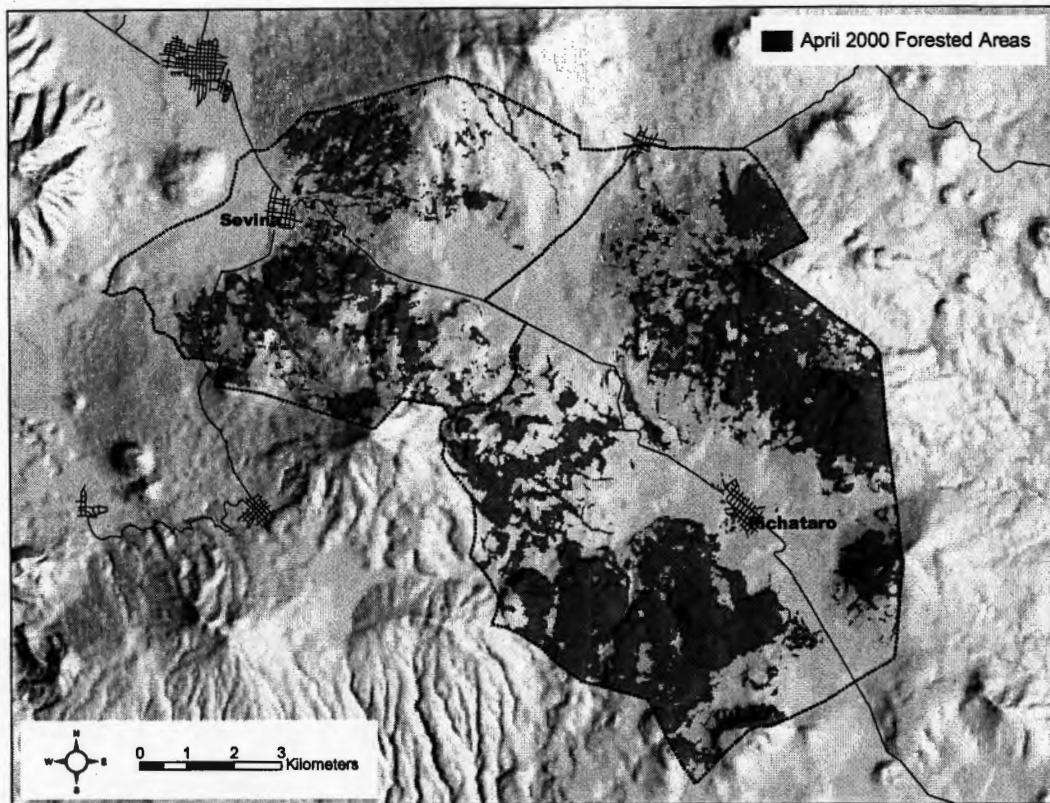
Figure 4.2. April 2000 ETM+ image land-cover classification of total forest extent.

Table 4.2. Error matrix from accuracy assessment of 2000 ETM+ supervised classification.

	Reference Data		
Classified Data	Non-Forest	Forest	Row Totals
Non-Forest	27	3	30
Forest	1	29	30
Column Totals	28	32	60

	Producer's Accuracy	User's Accuracy
Non-Forest	96.4%	90.0%
Forest	90.6%	96.7%

Overall Accuracy:	93.3%	
KAPPA:	0.867	

I performed a comparison of the forest management areas of Sevina and Pichátaro by summarizing the results of the supervised classification for the two communities (Table 4.3). Pichátaro is currently more forested in both absolute and relative terms, with approximately three times the forested area as Sevina, and an 18% greater portion of its communal land identified as forested in 2000. Pichátaro also has a higher number of forested acres relative to its population—0.79 ha of forested land per person versus 0.48 ha/person within the community of Sevina (Table 4.4).

Table 4.3. Summary of 2000 forested areas by community.

	Pichátaro		Sevina		Totals	
	Area (ha)	% of total area	Area (ha)	% of total area	Area (ha)	% of total area
Forested	3,934.40	45.7%	1,299.50	27.6%	5,233.90	39.3%
Non-Forested	4,674.99	54.3%	3,413.40	72.4%	8,088.39	60.7%
Totals	8,609.40		4,712.90		13,322.29	

Table 4.4. 2000 forest distribution by community population.

	Pichátaro	Sevina	Totals
Estimated population[1]	5,000	2,700	7,700
Forested area (ha)	3,934.40	1,299.50	5,233.90
Forested hectares/person	0.79	0.48	0.68

[1] population estimates based on 2000 INEGI digital topographic data

Forest Change Since 1976

Automated Change Detection Results

The automated change detection resulted in maps of forest change for both sets of image dates (Figure 4.3). Both the 1976 to 1986 and the 1986 to 2000 change classifications have an overall accuracy of greater than 80%, with the Kappa coefficients differing significantly between the sensors (Table 4.6).

The results of the change detection show significant differences in the rate and extent of forest change between the communities of Sevina and Pichátaro. Between 1976 and 1986, both communities had a net overall gain in the amount of forested land (Table 4.5). Sevina in particular experienced a high rate of forest regrowth, gaining >200% of the forest cover it lost to deforestation. Between 1986 and 2000 Pichátaro continued to experience an overall net gain in forested area while Sevina's forests suffered a dramatic decline, losing >245 ha in this 14-year period (Table 4.7). In the period between 1986 and 2000, 93% of the deforestation in the combined study area occurred within the community boundary of Sevina, which manages ~35% of the study area. Only 21% of the regrowth occurred in Sevina in the same period.

Table 4.5. Summary of 1976 to 1986 automated change detection results.

	Pichátaro	Sevina	Study Area
Forest clearing (ha)	121.99	70.79	192.78
Forest regrowth (ha)	199.90	158.28	358.18
Net Change	77.91	87.49	165.40

64
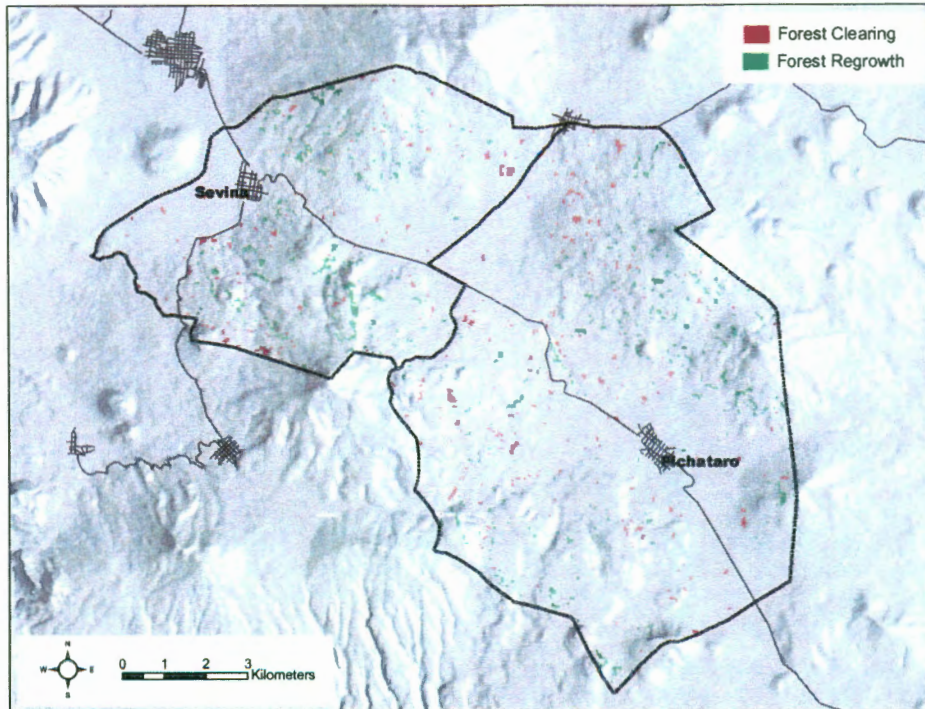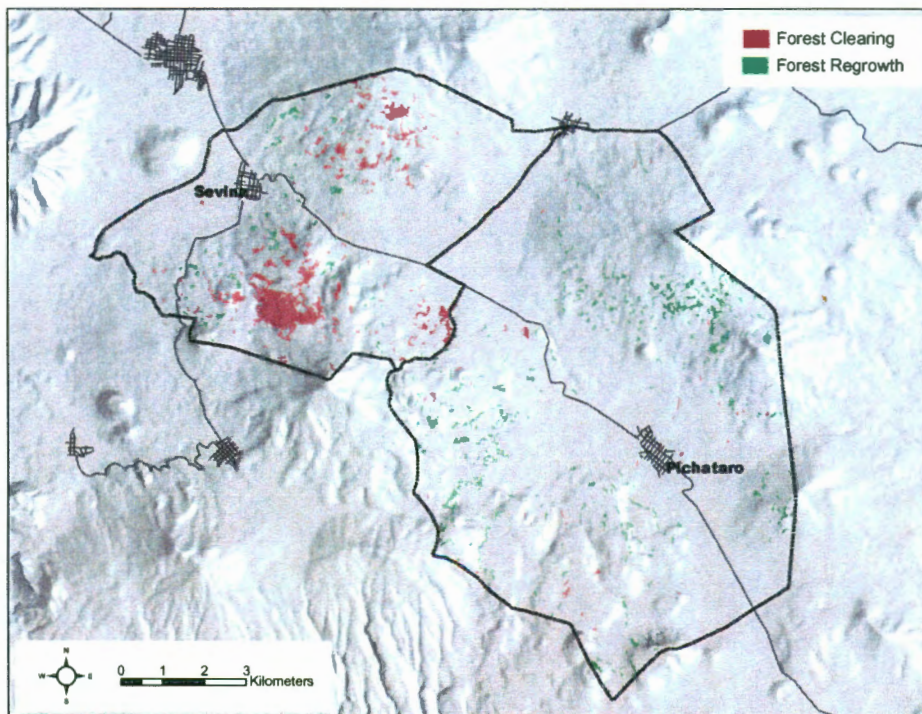
Figure 4.3. 1976 to 1986 (a) and 1986 to 2000 (b) forest change classifications.

Table 4.6. Error matrix from final accuracy assessment of 1986 to 2000 and 1976 to 1986 forest change classifications.

1986 to 2000 Difference Image

	Reference Data			
Classified Data	Cleared	No Change	Regrown	Row Totals
Cleared	30	2	0	32
No Change	3	49	4	56
Regrown	0	11	26	37
Column Totals	33	62	30	125

	Producer's Accuracy	User's Accuracy
Cleared	90.9%	93.8%
No Change	79.0%	87.5%
Regrown	86.7%	70.3%

Overall	
Accuracy:	84.0%
KAPPA:	0.750

1976 to 1986 Difference Image

	Reference Data			
Classified Data	Cleared	No Change	Regrown	Row Totals
Cleared	4	7	0	11
No Change	0	115	3	118
Regrown	0	19	16	35
Column Totals	4	141	19	164

	Producer's Accuracy	User's Accuracy
Cleared	100.0%	36.4%
No Change	81.6%	97.5%
Regrown	84.2%	45.7%

Overall	
Accuracy:	82.3%
KAPPA:	0.502

66
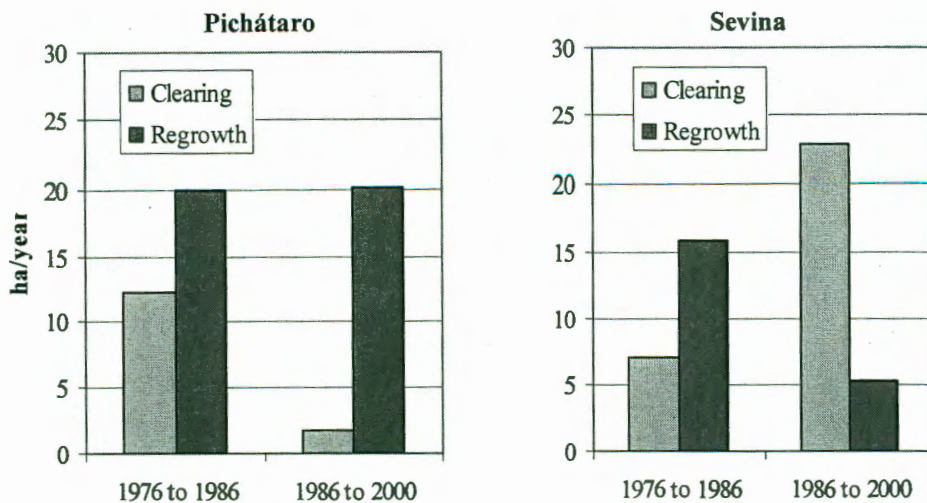
Figure 4.4. Average rates of forest clearing and regrowth in Pichátaro and Sevina between 1976 and 2000.

Table 4.7. Summary of 1986 to 2000 automated change detection results.

	Pichátaro	Sevina	Study Area
Forest clearing (ha)	24.13	320	344.14
Forest regrowth (ha)	281.24	74.12	355.36
Net Change	257.11	-245.88	11.23

Rates of forest clearing and regrowth also differed between the two communities (Table 4.8). The rate of clearing in the communal forests of Pichátaro dropped from an average of 12.2 ha/year between 1976 and 1986 to 1.72 ha/year between 1986 and 2000, a decrease of more than 85% (Figure 4.4). Sevina's average rate of clearing rose more than 222% between the same image periods, from 7.08 ha/year between 1976 and 1986 to 22.86 ha/year between 1986 and 2000. The overall loss of forest in Sevina

between 1986 and 2000 was made more dramatic by a 67% decline in the rate of

forest regrowth in comparison to the period between 1976 and 1986.

Table 4.8. Average rates of forest change in Sevina and Pichátaro between 1976 and 2000.

		Pichátaro		Sevina	
Image Dates	Number of years	Area (ha) cleared/year	Area (ha) regrown/year	Area (ha) cleared/year	Area (ha) regrown/year
1976 to 1986	10	12.20	19.99	7.08	15.83
1986 to 2000	14	1.72	20.09	22.86	5.29
Percent Change		-85.9%	0.5%	222.9%	-66.6%

	Combined Study Area		
Image Dates	Number of years	Area (ha) cleared/year	Area (ha) regrown/year
1976 to 1986	10	19.28	35.82
1986 to 2000	14	24.58	25.38
Percent Change		-85.9%	0.5%

Temporal Classification of Forest Extent

The temporal classification produced maps of forest extent in 1976 (Figure 4.5a)

and 1986 (Figure 4.5b). Accuracy assessment of the images generated relatively high

Kappa coefficients, 0.867 and .0967, respectively (Table 4.9).

Overall differences in forest extent between 1976 and 1986 show Sevina and

Pichátaro as having net increases in forest cover of 2.2% and 6.0%, respectively.

(Table 4.10). However, between 1986 and 2000 Pichátaro continued to experience a

net gain while Sevina cleared ~16% of its total forested land (Figure 4.6).
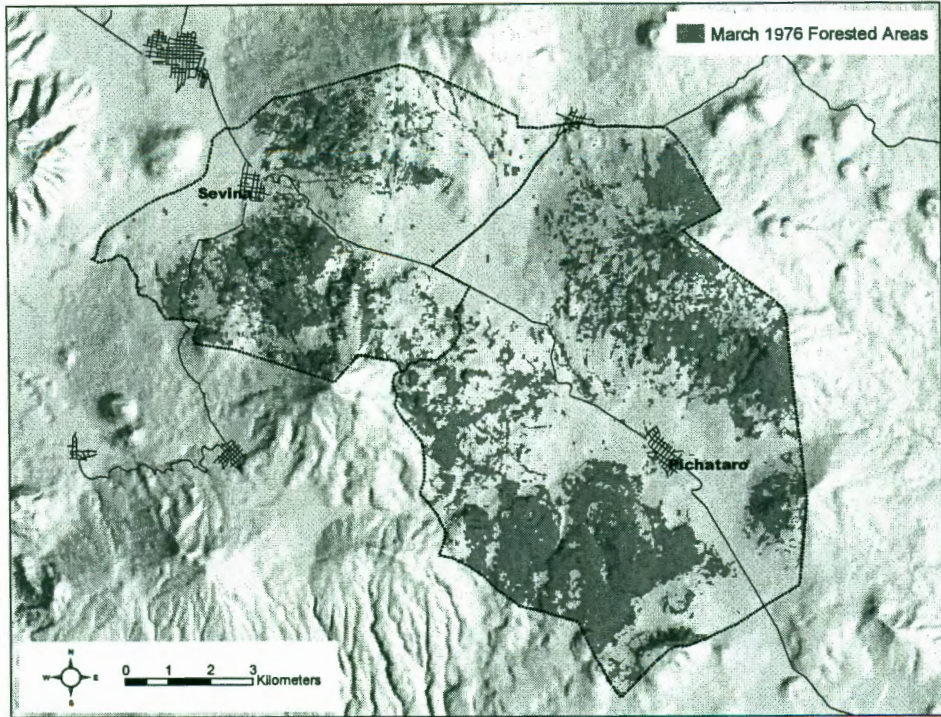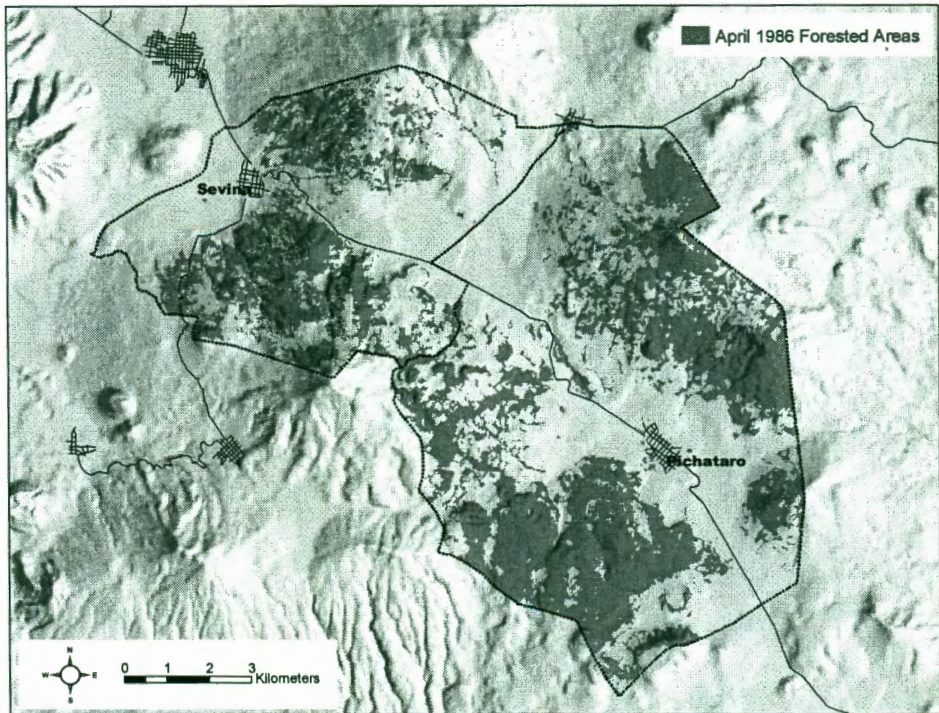
Figure 4.5. Temporally-classified forest extent in 1976 (a) and 1986 (b).

Table 4.9. Error matrix from final accuracy assessment of 1986 and 1976 temporal classification images.

Temporally classified 1986 Image

	Reference Data		
Classified Data	Non-Forest	Forest	Row Totals
Non-Forest	29	1	30
Forest	0	30	30
Column Totals	29	31	60

	Producer's Accuracy	User's Accuracy
Cleared	100.0%	96.7%
Not Cleared	96.8%	100.0%

Overall Accuracy:	98.3%
KAPPA:	0.967

Temporally-classified 1976 Image

	Reference Data		
Classified Data	Non-Forest	Forest	Row Totals
Non-Forest	27	3	30
Forest	1	29	30
Column Totals	28	32	60

	Producer's Accuracy	User's Accuracy
Cleared	96.4%	90.0%
Not Cleared	90.6%	96.7%

Overall Accuracy:	93.3%
KAPPA:	0.867
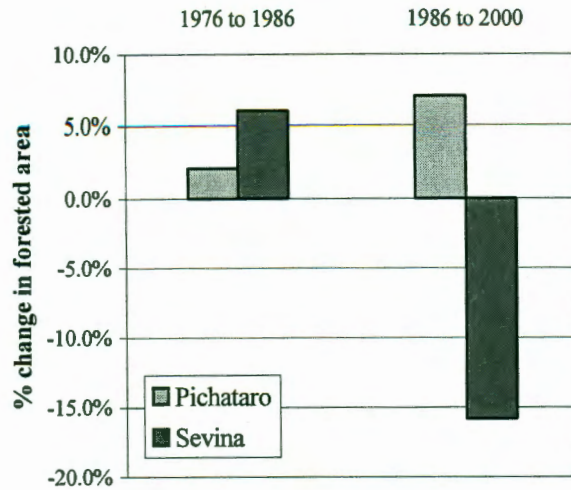
Figure 4.6. Net change in forested area from 1976 to 1986 and 1986 to 2000.

Table 4.10. Total forest extent in 1976, 1986 and 2000.

	Pichátaro		Sevina		Study Area	
	Area (ha)	% Change	Area (ha)	% Change	Area (ha)	% Change
1976	3,597.80		1,456.09		5,053.89	
1986	3,675.71	2.2%	1,543.58	6.0%	5,219.30	3.3%
2000	3,934.40	7.0%	1,299.50	-15.8%	5,233.90	0.3%

1976 to 2000 Forest Change Trajectories

The map of forest change trajectories is useful for identifying both spatial and temporal changes in the two communities (Figure 4.7). Much of the recent clearing (since 1986) appears to be concentrated around the summit of El Iriepu in the south-central portion of Sevina's jurisdiction, with other large patches of clearing along the slopes of El Capen, also in Sevina. Pichátaro, however, has larger patches of both

71
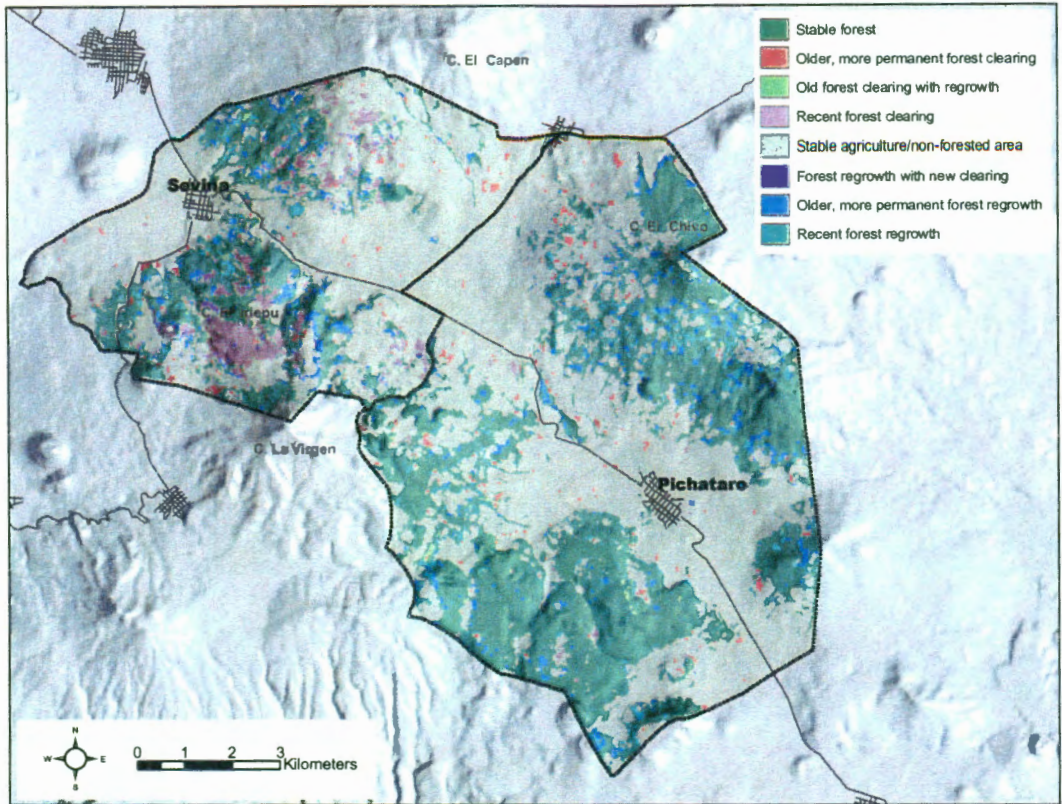
Figure 4.7. March 1976 to April 2000 forest cover change trajectories.

older and more recent regrowth, mostly near the summit of El Chivo. A summary of the change trajectories shows the differences between the two communities (Table 4.11). Pichátaro has a higher proportion of forest that was stable through the 1976 to 2000 time period (~40%) than neighboring Sevina (~23%).

The change trajectories suggest that most of the differences in the forested lands managed by these two communities have arisen since the late 1980s (Figure 4.8). This also supports other findings that, prior to 1986, the management and harvesting

Table 4.11. Summary of forest change trajectories within the study area.

Change trajectory category	Pichátaro		Sevina	
	hectares	% of area	hectares	% of area
Stable Forest	3,453.75	40.2%	1,091.49	23.2%
Older, more permanent forest clearing	102.89	1.2%	62.56	1.3%
Old forest clearing with regrowth	19.08	0.2%	8.19	0.2%
Recent forest clearing	22.06	0.3%	293.81	6.2%
Stable agriculture/non-forested area	4,541.71	52.8%	3,028.63	64.3%
Forest regrowth with new clearing	2.07	0.0%	26.19	0.6%
Older, more permanent forest regrowth	197.83	2.3%	132.09	2.8%
Recent forest regrowth	261.69	3.0%	65.86	1.4%
TOTALS	8,601.10		4,708.82	

Change trajectory category	Study Area	
	hectares	% of area
Stable Forest	4,545.64	34.1%
Older, more permanent forest clearing	165.47	1.2%
Old forest clearing with regrowth	27.27	0.2%
Recent forest clearing	315.88	2.4%
Stable agriculture/non-forested area	7,570.87	56.9%
Forest regrowth with new clearing	28.26	0.2%
Older, more permanent forest regrowth	329.94	2.5%
Recent forest regrowth	327.58	2.5%
TOTALS	13,310.92	

practices employed by Sevina and Pichátaro appear to have been much more similar (Works and Hadley, 2004).

Landscape Metrics

The landscape metrics also show differences between the two communities, again concentrated in the period between 1986 and 2000 (Table 4.12). While Pichátaro's overall percentage of forest increased slightly, Sevina's dropped from 32.72% to 27.55%. In the same period, Sevina experienced a decrease in the mean forest patch
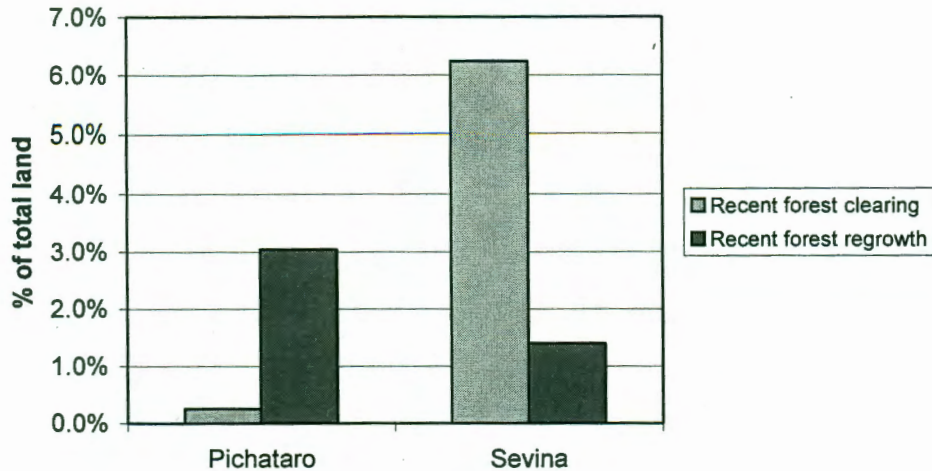
Figure 4.8. Clearing and regrowth since 1986 (as a percentage of total land.)

size (9.22 to 6.71) and largest-patch index (18.67 to 10.71), while increasing the total number of patches (168 to 195) and the mean Euclidean nearest-neighbor distance (94.30 to 100.32). The metrics suggest a more isolated, fragmented forest in Sevina than in the period before 1986. The 1976 results indicate a more fragmented forest in both communities than in 1986, with a large number of small, relatively isolated patches. The 1976 metrics support my earlier findings that the period between 1976 and 1986 was one primarily of forest regrowth. It is possible that the forests of the region were regenerating from a period of relatively high deforestation in the years before 1976.

Table 4.12. Summary of landscape metrics for 1976, 1986, and 2000 land-cover classification images (see to Table 3.17 for a description of the metrics).

1976 Classification Image

Pichátaro

TYPE	PLAND	LPI	NP	MPS	ED	MSI	MENN
Non-Forested	58.18	49.19	290.00	17.30	69.18	1.34	87.85
Forested	41.82	20.92	349.00	10.33	71.61	1.35	96.12

Sevina

TYPE	PLAND	LPI	NP	MPS	ED	MSI	MENN
Non-Forested	69.14	64.14	214.00	15.30	81.40	1.34	74.13
Forested	30.86	15.88	258.00	5.67	83.30	1.41	96.74

1986 Classification Image

Pichátaro

TYPE	PLAND	LPI	NP	MPS	ED	MSI	MENN
Non-Forested	57.26	48.69	273.00	18.08	60.68	1.35	88.47
Forested	42.74	20.92	276.00	13.35	63.29	1.38	93.32

Sevina

TYPE	PLAND	LPI	NP	MPS	ED	MSI	MENN
Non-Forested	67.28	55.49	268.00	11.89	76.18	1.33	72.83
Forested	32.72	18.67	168.00	9.22	78.17	1.53	94.30

2000 Classification Image

Pichátaro

TYPE	PLAND	LPI	NP	MPS	ED	MSI	MENN
Non-Forested	54.31	47.12	266.00	17.66	49.21	1.27	102.56
Forested	45.69	22.37	218.00	18.12	51.89	1.34	102.16

Sevina

TYPE	PLAND	LPI	NP	MPS	ED	MSI	MENN
Non-Forested	72.45	69.11	149.00	23.11	58.05	1.26	76.76
Forested	27.55	10.71	195.00	6.71	60.00	1.41	100.32

Table 4.13. Summary of landscape metrics for forest change trajectory images (see Table 3.17 for a description of the metrics.)

Pichátaro

Change trajectory	PLAND	LPI	NP	MPS	ED	MSI	MENN
Stable Forest	40.16	20.26	311.00	11.13	65.04	1.38	92.50
Older, more permanent forest clearing	1.20	0.05	175.00	0.59	6.74	1.09	300.62
Old forest clearing with regrowth	0.22	0.03	48.00	0.40	1.74	1.19	431.54
Recent forest clearing	0.26	0.04	42.00	0.53	1.90	1.26	493.65
Stable agriculture/non-forested area	52.80	45.94	285.00	15.97	56.50	1.28	100.06
Forest regrowth with new clearing	0.02	0.01	7.00	0.30	0.23	1.16	767.21
Older, more permanent forest regrowth	2.30	0.06	280.00	0.71	12.82	1.14	188.19
Recent forest regrowth	3.04	0.12	344.00	0.76	19.69	1.35	129.62

Sevina

Change trajectory	PLAND	LPI	NP	MPS	ED	MSI	MENN
Stable Forest	23.16	8.85	253.00	4.33	64.49	1.40	93.32
Older, more permanent forest clearing	1.40	0.11	94.00	0.70	9.16	1.30	198.48
Old forest clearing with regrowth	0.55	0.07	69.00	0.38	4.13	1.12	240.26
Recent forest clearing	6.22	2.63	158.00	1.86	23.52	1.38	150.76
Stable agriculture/non-forested area	64.38	53.86	276.00	11.04	80.56	1.29	75.53
Forest regrowth with new clearing	1.32	0.08	110.00	0.57	7.53	1.08	284.65
Older, more permanent forest regrowth	2.80	0.14	184.00	0.72	15.60	1.16	161.91
Recent forest regrowth	0.17	0.05	16.00	0.51	1.04	1.11	766.30

Results were similar for the forest change trajectory metrics (Table 4.13). Sevina's relatively large largest-patch index (2.63), mean patch size (1.86), and number of patches (158) in the 'recent clearing' category relative to Pichátaro (0.04, 0.53, and 42, respectively) indicate that large areas of Sevina's forest are being cleared. These areas

are in relatively close proximity to one another as indicated by the low MENN of 150.76, versus 493.65 for Pichátaro. Conversely, Sevina's forest regrowth patches are small, few in number and relatively isolated, with a MENN of 766.36. Pichátaro has been more successful at protecting recent regrowth, with only a few, isolated areas being cleared from 1986 to 2000. In the same period, Sevina lost 110 patches of recently grown forests averaging 0.57 ha in size. This again suggests that the differences between the two communities are a relatively recent phenomena.

CHAPTER 5: CONCLUSIONS

The primary objective of my study was to use satellite imagery and automated change detection to map forest change in the study area since 1976. The accuracy assessment of the change detection images indicate that I was able to accurately identify these areas of forest change. I also mapped the historic extent of forested land-cover using the most current forest conditions, represented by the 2000 land-cover classification, as reference. Accuracy assessments indicate that this mapping was successful as well. This type of temporal-classification is useful because it facilitates the creation of additional maps for past or future image dates with relatively minimal processing. For example, the areas of forest clearing and forest regrowth can be identified in a 2004 Landsat ETM+ image using the automated change detection methodology employed by my study. A map of overall forest extent in 2004 is then created using the April 2000 map of forest extent as reference.

My second objective was to compare the differences in the rate and extent of forest change in the communities of Sevina and Pichátaro. The change detection analysis and change trajectory mapping reveals differences in the rates of deforestation and forest regrowth between the two communities. While the forest resources of both communities remained more or less stable in the period between 1976 and 1986, deforestation in Sevina increased sharply between 1986 and 2000. Sevina's rate of forest regrowth also dropped in the same period, exacerbating the problem of forest decline. The differences in the two communities appear related to their forest

78

management practices (Works and Hadley, 2004). Pichátaro has primarily focused on local processing of wood resources. Sevina's reliance on exporting unprocessed timber has forced it to rely on larger-scale, clear-cut style harvesting to derive economic benefit from its forests (Works and Hadley, 2004). This type of management is not sustainable given the relatively small forested area managed by each community. In Sevina's case it has led to a rapid and severe degradation of its forests.

It is tempting to conclude that Sevina simply needs to adopt Pichátaro's management and production style. However, the supply of the type of wood products created by the Meseta's craftspeople may already exceed demand. A visit to any of the many local markets that sell these goods reveals a large supply of locally produced wood furniture and carvings. Certain items, such as carved wood boxes, are ubiquitous, with little variety to differentiate them from one another. In the case of Pichátaro, the focus of furniture production appears to be primarily on high productivity and low to intermediate quality products. Little high-grade furniture is currently being produced. This may be a consequence of the heavy reliance on foreign and domestic tourists as the primary consumers of these products, the lack of highly skilled craftspeople, and the absence of economic incentive to produce higher quality goods. Sevina's orientation toward the western Meseta has left it largely excluded from this market (Works and Hadley, 2004). A coordinated effort by Sevina to gain a larger share of the tourism economy could result in increased competition for customers. Lower prices would likely result, leading to a diminished economic return for all locally-produced timber products. Production may subsequently increase as

79

people struggle to earn the same income in a climate of lower prices, resulting in a higher rate of forest harvesting and wood resource consumption.

Change detection successfully identified overall changes in forest extent but did not provide information on changes in forest structure, health, or composition. Field data show that all stands in the study area have been heavily impacted by human activity. Few large pines have been spared harvest and young pines are often being harvested as soon as they achieve a commercially-viable size (Chase, 2003). Severe soil erosion appears widespread and problematic. These impacts may not be reversible in the short-term, despite recent replanting efforts. Though these conditions are present in both communities, they appear more severe in Sevina's management area. Furthermore, while areas of forest regrowth were identified by the change detection, it is difficult to assess without additional field study whether the composition of this regrowth is the same as the original forests of the region. Some regrowth is oak or alder dominated, for example, making it less valuable to the local economy (Works and Hadley, 2001). It is also difficult to assess how selective harvesting has affected the areas that were classified as unchanged. Many areas may have transitioned from relatively pure pine stands to a mixture of pine, oak, alder and fir, thus reducing their economic value. The forests of the Meseta are probably much more degraded than the results of this study suggest. Commercially valuable pine appears to be disappearing at a rapid rate in both communities (Chase, 2003; Works and Hadley, 2004).

Extensions of this research would include additional Landsat imagery since 1976 to better quantify changes in the rates and patterns of deforestation from year to year.

Given the high rate of forest change in the study area, more recent imagery is needed to map current forest extents. A simple and cost effective effort to monitor changes in forests at regular intervals, such as semi-annually, would also be possible using my methodology. Although the accuracy of the resulting maps would decrease as image dates become further removed from the April 2000 reference classification, the results of my study suggest it could be several decades before the temporal classification accuracy decreases to the point that a new reference image date is needed. This could have implications in other long-term change detection studies that rely on satellite image analysis. If the primary objective of a study is to identify general areas of forest change, it may be more cost effective to focus field data collection on a single image date to establish a high-quality reference classification. Subsequent image dates can be temporally-classified, thereby avoiding the costs of additional field work.

A major limitation of this study was my inability to identify specific forest types. This is an issue in many change detection studies but especially problematic in the Meseta because of the exclusivity of pine as the main economic resource. The ability to identify where pine dominated stands are being replaced by a mixture of other species would help local jurisdictions be more effective in their forest management policies. These areas could be targeted for replanting and protection. A second, smaller field effort could effectively refine the training areas and increase the sample size for some of the under-represented classes. This might allow classification of forest based on composition using the supervised methodology described in my study. Another option would be the use of higher-resolution satellite imagery such as SPOT

81

or IKONOS. A smaller pixel size would decrease the mixing of multiple stand types in a single pixel, reducing the confusion between forest classes and increasing the possibility of a more sophisticated classification (Read, 2003). However, using higher resolution satellite imagery currently requires more comprehensive field data collection and training area selection (Chen and Stow, 2002). Given one of the main advantages of using remotely sensed data is the efficiency of processing, this is a significant limitation. As new techniques are developed for the classification of higher resolution imagery, analytical complexity should decrease, making this a viable option in the future. A more immediate alternative may be hyperspectral imagery. Traditional multi-spectral imagery, such as Landsat ETM+, contains a few relatively broad wavelength bands. Hyperspectral sensors can collect image data in dozens or even hundreds of narrow, adjacent spectral bands. The increased spectral resolution of hyperspectral imagery increases the likelihood of land-cover exhibiting a unique spectral signature, improving the accuracy of supervised classification (Jensen, 1996; Mustard and Sunshine, 1999).

A more difficult task would be to develop a systematic technique for mapping changes in the individual forest categories over time (e.g., mixed pine to mixed oak to cleared). The change detection and temporal classification used by my study is only applicable to a single land-cover class, i.e., identifying overall changes in forest extent. It might be possible to modify the Kappa thresholding to identify areas where the forest has changed from one stand type to another between two image dates, but it

would most likely involve a large number of thresholding operations and would significantly increase the complexity of the analysis.

As the use of satellite imagery for land-cover change detection becomes increasingly widespread, we can look forward to more sophisticated and robust techniques that will be able to address its current limitations. These improved change detection methods would be extremely helpful for the mapping, monitoring, and managing of rapidly changing landscapes such as the diminishing forests of Meseta Purépecha.

REFERENCES CITED

Alvarez-Icaza, P., G. Cervera, C. Garibay, P. Guitierrez, and F. Rosete, 1993. *Los Umbrales del Deterioro : La Dimension Ambiental de un Desarollo Desigual en la Region Purépecha.* Fundacion Friedrich Ebert, Mexico, D.F., Mexico.

Campbell, J.B., 1996. *Introduction to Remote Sensing.* Guilford Press, New York, New York, 622 p.

Chase, J.C., 2003. *Forest Landscape Change in the Meseta Purépecha, Michoacán, Mexico.* Unpublished Master's thesis, Department of Geography, Portland State University, Portland, Oregon, 106 p.

Chen, D., and D. Stow, 2002. The effect of training strategies on supervised classification at different spatial resolutions, *Photogrammetric Engineering & Remote Sensing,* 68(11):1155-1161.

Civco, D.L., 1989. Topographic normalization of thematic mapper digital imagery, *Photogrammetric Engineering & Remote Sensing,* 55(9):1303-1309.

Cohen, W.B., M. Fiorella, G. Gray, E. Helmer, and K. Anderson, 1998. An efficient and accurate method for mapping forest clearcuts in the Pacific Northwest using Landsat imagery, *Photogrammetric Engineering & Remote Sensing,* 64:293-300.

Cohen, W.B, T.A. Spies, and M. Fioralla, 1995. Estimating the age and structure of forests in a multi-ownership landscape of western Oregon, U.S.A., *International Journal of Remote Sensing,* 16(4):721-746.

Colby, J.D., 1991. Topographic normalization in rugged terrain, *Photogrammetric Engineering & Remote Sensing,* 57(5):531-537.

Colby, J.D., and P.L. Keating, 1998. Land-cover classification using Landsat TM imagery in the tropical highlands: the influence of anisotropic reflectance, *International Journal of Remote Sensing,* 19(8):1479-1500.

Congalton, R.G., and K. Green, 1999. *Assessing the Accuracy of Remotely Sensed Data: Principles and Practices.* Lewis Publishers, New York, New York, 137 p.

Eckhardt, D.W., J.P. Verdin, and G.R. Lyford, 1990. Automated update of an irrigated lands GIS using SPOT HRV imagery, *Photogrammetric Engineering & Remote Sensing,* 56(11):1515-1522.

ERDAS, 1999. *ERDAS Field Guide, Fifth Edition.* ERDAS, Inc., Atlanta, Georgia, 698 p.

Frohn, R.C., 1998. *Remote Sensing for Landscape Ecology: New Metric Indicators for Monitoring, Modeling, and Assessment of Ecosystems.* Lewis Publishers, Boca Raton, Florida, 99p.

Fung, T. and E. LeDrew, 1988. The Determination of Optimal Threshold Levels for Change Detection Using Various Accuracy Indices, *Photogrammetric Engineering & Remote Sensing,* 54(10):1449-1454.

Garcia, M.C., and R. Alvarez, 1994. TM digital processing of a tropical forest region in southwestern Mexico, *International Journal of Remote Sensing,* 15(8):1611-1632.

Hadley, K.S. and M. Savage, 1996. Wind disturbance and development of a near-edge forest interior, Marys Peak, Oregon Coast Range, *Physical Geography,* 17:47-61.

Hale, S.R., and B.N. Rock, 2003. Impact of topographic normalization on land-cover classification accuracy, *Photogrammetric Engineering & Remote Sensing,* 69(7):785-791.

Hall, F.G., D.E. Strebel, J.E. Nickenson, and S.J. Goetz, 1991. Radiometric rectification: Toward a common radiometric response among multidate, multisensor images, *Remote Sensing of Environment,* 35(1):11-27.

Hayes, D.J., and S.A. Sader, 2001. Comparison of change-detection techniques for monitoring tropical forest clearing and vegetation regrowth in a time series, *Photogrammetric Engineering & Remote Sensing,* 67(9):1067-1075.

Jaffee, D.S., 1996. *Confronting Globalization in the Community Forests of Michoacan, Mexico: Free Trade, Neoliberal Reforms, and Resource Degradation.* Unpublished Master's thesis, Department of Environmental Studies, University of Wisconsin, Madison, 84 p.

Jenson, J.R., 1996. *Introductory Digital Image Processing,* Prentice-Hall, Englewood Cliffs, New Jersey, 316 p.

Jensen, J.R., K. Rutchey, M.S. Koch, and S. Narumalani, 1995. Inland wetland change detection in the Everglades Water Conservation area 2A using a time series of normalized remotely sensed data, *Photogrammetric Engineering & Remote Sensing,* 61(2):199-209.

Keating, P.L., 1997. Mapping vegetation and anthropogenic disturbances in southern Ecuador with remote sensing techniques: implications for park management, *Yearbook: Conference of Latin American Geographers*, 23:77-90.

Kelly, M., D. Shaari, Q. Guo, and D. Liu, 2004. A comparison of standard and hybrid classifier methods for mapping hardwood mortality in areas affected by "sudden oak death", *Photogrammetric Engineering & Remote Sensing*, 70(11):1229-1239.

Landis J.R., and G.G. Koch, 1977. The Measurement of Observer Agreement for Categorical Data, *Biometrics*, 33:159-174.

Leprieur, C., J. Durrand, and J. Peyton, 1988. Influence of topography on forest reflectance using Landsat Thematic Mapper and digital terrain data, *Photogrammetric Engineering & Remote Sensing*, 54(4):491-496.

Lunetta, R., J. Lyon, J. Sturdevant, J. Dwyer, C. Elvidge, D. Yuan, L. Fenstermaker, S. Hoffer, and R Weerackroon, 1993. *North American Landscape Characterization (NALC-Pathfinder) Project Research Plan,* U.S Environmental Protection Agency report EPA/600/R-93/135, 427 p.

Lyon, J.G., D. Yuan, R.S. Lunetta, and C.D. Elvidge, 1998. A Change Experiment Using Vegetation Indices, *Photogrammetric Engineering & Remote Sensing*, 64(2):143-150.

Macleod, R.D., and R.G. Congalton, 1998. A quantitative comparison of change detection algorithms for estimation of land surface parameters, *Photogrammetric Engineering & Remote Sensing*, 64(2):207-216.

Mas, J.F., 1999. Monitoring land-cover changes: a comparison of change detection techniques, *International Journal of Remote Sensing*, 20(1):139-152.

Mas, J.F., and I. Ramirez, 1996. Comparison of land use classifications obtained by visual interpretation and digital processing, *ITC Journal*, 3-4:278-283.

McGarigal, K. and B.J. Marks, 1994. *Fragstats: Spatial pattern analysis program for quantifying landscape structure, v 2.0.* Oregon Forest Science Lab, Oregon State University, Corvallis, Oregon, 141 p.

Mertens, B., and E.F. Lambin, 1997. Spatial modeling of deforestation in Southern Cameroon, *Applied Geography*, 17: 143-162.

Mertens, B., and E.F. Lambin, 2000. Land-cover-change trajectories in Southern Cameroon, *Annals of the Association of American Geographers*, 90(3): 467-495.

Minneart, M., 1941. The repricocity principle in lunar photometry, *Astrophysical Journal*, 93:403-410.

Mustard, J. F., and J.M. Sunshine, 1999. Spectral analysis for Earth Science: investigations using remote sensing data. In: *Remote Sensing for the Earth Sciences: Manual of Remote Sensing (3rd ed.)*, A.N. Renz, Ed., John Wiley & Sons, New York, 251-306.

Oderwald, R.G., and R.H. Wynne, 2000. Field applications for statistical data and techniques, *Journal of Forestry*, 98(6):58-60.

Perry, Jr., J.P., 1991. *The Pines of Mexico and Central America*. Timber Press, Portland, Oregon, 231 p.

Pilon, P.G., P.J. Howarth, and R.A. Bullock, 1988. An enhanced classification approach to change detection in semi-arid environments, *Photogrammetric Engineering & Remote Sensing*, 54(12):1709-1716.

Read, J.M., 2003. Spatial analyses of logging impacts in Amazonia using remotely sensed data, *Photogrammetric Engineering & Remote Sensing*, 69(3):275-282.

Refan, M.H. and K. Mohammadi, 2001. *Point averaging of GPS position components, before and after Selective Availability*. Paper presented at the 2001 Asian GPS Conference, New Delhi, India.

Ritters, K.H., R.V.O. O'Neill, C.T. Hunsaker, J.D. Wickham, D.H. Yankee, S.P. Timmons, K.B. Jones, and B.L. Jackson, 1995. A factor analysis of landscape pattern and structure metrics, *Landscape Ecology*, 10:23-39.

Rosenfield, G.H., and K. Fitzpatrick-Lins, 1986. A Coefficient of Agreement as a Measure of Thematic Classification Accuracy, *Photogrammetric Engineering & Remote Sensing*, 49(9):1303-1314.

Running, SW., D.L. Peterson, M.A. Spanner, and K.B. Teuber, 1986. Remote sensing of coniferous forest leaf area, *Ecology*, 67(1):273-276.

Smith, J.A., and T.L. Lin, 1980. The Lambertian assumption and Landsat data, *Photogrammetric Engineering & Remote Sensing*, 46:1183-1189.

Southworth, J., and C. Tucker, 2001. The influence of accessibility, local institutions, and socioeconomic factors on forest cover change in the mountains of western Honduras, *Mountain Research and Development*, 21(3): 276-283.

APPENDIX: SATELLITE DATA SOURCES

Landsat 2 Multi-Spectral Scanner (MSS) Scene. March 28, 1976. WRS Path 28, Row 46. Acquisition Time: 16:24. Projection: UTM zone 14-north, NAD27 datum. Resolution: 60m. USGS EROS Data Center—North American Landscape Characterization (NALC) project.

Landsat 5 Multi-Spectral Scanner (MSS) Scene. April 6, 1986. WRS Path 28, Row 46. Acquisition Time: 16:37. Projection: UTM zone 14-north, NAD27 datum. Resolution: 60m. USGS EROS Data Center—North American Landscape Characterization (NALC) project.

Landsat 5 Thematic Mapper (TM) Scene. April 6, 1986. WRS Path 28, Row 46. Acquisition Time: 16:37. Projection: UTM zone 14-north, WGS84 datum. Resolution: 30m (120m thermal). USGS EROS Data Center.

Landsat 7 Enhanced Thematic Mapper Plus (ETM+) Scene. April 20, 2000. WRS Path 28, Row 46. Acquisition Time: 17:04. Projection: UTM zone 14-north, WGS84 datum. Resolution: 30m (15m panchromatic, 60m thermal). USGS EROS Data Center.